bioRxiv preprint doi: https://doi.org/10.1101/2024.03.22.586274; this version posted October 8, 2024. The copyright holder for this preprint (which was not certified by peer review) is the author/funder, who has granted bioRxiv a license to display the preprint in perpetuity. It is made available under aCC-BY 4.0 International license.

**Title:**

# Base editing of *Ptbp1* in neurons alleviates symptoms in a mouse model of Parkinson's disease

**Authors:**

Desirée Böck[1,#,*], Maria Wilhelm[1,#], Jonas Mumenthaler[1], Daniel Fabio Carpanese[1], Peter I. Kulcsár[1], Simon d'Aquin[1], Alessio Cremonesi[2], Anahita Rassi[2], Johannes Häberle[3], Tommaso Patriarchi[1,4*], Gerald Schwank[1,*]

[#]These authors contributed equally.

[*]Correspondence: patriarchi@pharma.uzh.ch; schwank@pharma.uzh.ch; desiree.boeck@uzh.ch

**Affiliations:**

[1]Institute of Pharmacology and Toxicology, University of Zurich, Zürich, Switzerland

[2]Division of Clinical Chemistry and Biochemistry, University Children's Hospital Zurich, University of Zurich, Zurich, Switzerland

[3]Division of Metabolism and Children's Research Center, University Children's Hospital Zurich, Zurich, Switzerland

[4]Neuroscience Center Zurich, University of Zurich and ETH Zurich, Zurich, Switzerland

**Abstract**

Parkinson's disease (PD) is a multifactorial disease caused by irreversible progressive loss of dopaminergic neurons (DANs). Recent studies have reported successful conversion of astrocytes into DANs by repressing polypyrimidine tract binding protein 1 (PTBP1), which led to the rescue of motor symptoms in a chemically-induced mouse model of PD. However, several follow-up studies have questioned the validity of this astrocyte to DAN conversion model. In this study, we devised an adenine base editing strategy to downregulate PTBP1 in astrocytes and neurons in a chemically-induced PD mouse model. While PTBP1 downregulation in astrocytes had no effect, we observed that PTBP1 downregulation in neurons of the substantia nigra pars compacta and striatum resulted in the expression of the DAN marker tyrosine hydroxylase (TH) in non-dividing neurons, which was associated with an increase in striatal dopamine concentrations and a rescue of forelimb akinesia and spontaneous rotations. Phenotypic analysis using multiplexed iterative immunofluorescence imaging further revealed that most of the TH-positive cells in the striatum co-expressed the

bioRxiv preprint doi: https://doi.org/10.1101/2024.03.22.586274; this version posted October 8, 2024. The copyright holder for this preprint (which was not certified by peer review) is the author/funder, who has granted bioRxiv a license to display the preprint in perpetuity. It is made available under aCC-BY 4.0 International license.

dopaminergic marker DAT and the pan-neuronal marker NEUN, with the majority of these triple-positive cells being classified as mature GABAergic neurons. Additional research is needed to fully elucidate the molecular mechanisms underlying the expression of the observed markers and understand how the formation of these cells contributes to the rescue of spontaneous motor behaviors. Nevertheless, our findings support a model where neuronal, but not astrocytic, downregulation of PTBP1 can mitigate symptoms in PD mice.

## Introduction

Parkinson's disease (PD) is a complex and multifactorial disorder, characterized by the progressive and irreversible loss of dopaminergic neurons (DANs) in the substantia nigra pars compacta (SNc), which leads to the disruption of the nigrostriatal pathway and depletion of striatal dopamine (Bloem et al., 2021; Gitler et al., 2017; Moore et al., 2005). The cause of PD is unknown and only a handful of genetic and environmental risk factors have been identified (Brown et al., 2005; de Lau and Breteler, 2006; Elbaz et al., 2007; Kalia and Lang, 2015), making the development of a curative therapy challenging. In fact, current treatment strategies do not focus on slowing down or halting disease progression, but rather aim to control symptoms and maintain the patients' quality of life (Stoker and Barker, 2020).

Recently emerging *in vivo* transdifferentiation approaches, which leverage the plasticity of specific somatic cell types, hold great promise for developing therapies targeting a wide range of neurodegenerative diseases, including PD (Cohen and Melton, 2011; Torper and Götz, 2017). Astrocytes are of particular interest for such cell fate-switching approaches. First, they are non-neuronal cells and thus not affected by neurodegeneration (Yu et al., 2020). Second, they can acquire certain characteristics of neural stem cells, including multipotency, when activated (Niu et al., 2013; Buffo et al., 2008; Robel et al., 2011; Shimada et al., 2012; Sirko et al., 2013). Finally, they are highly proliferative upon brain injuries such as neurodegeneration (Yu et al., 2021). Several *in vivo* studies have reported successful reprogramming of astrocytes to neurons via overexpression of proneuronal lineage-specific transcription factors, such as NEUROD1 or SOX2 (Guo et al., 2014; Niu et al., 2015, 2013). Moreover, two recent studies have shown that repression of the RNA-binding protein polypyrimidine tract binding protein 1 (PTBP1), which mainly functions as a splicing regulator (Valcárcel and Gebauer, 1997), efficiently converts astrocytes into DANs in the SNc or striatum (Qian et al., 2020; Zhou et al., 2020). Consequently, this led to the restoration of the nigrostriatal pathway and striatal dopamine levels, as well as rescue of motor deficits in a chemically-induced mouse model of PD (Qian et al., 2020; Zhou et al., 2020). However, since the publication of these two studies

bioRxiv preprint doi: https://doi.org/10.1101/2024.03.22.586274; this version posted October 8, 2024. The copyright holder for this preprint (which was not certified by peer review) is the author/funder, who has granted bioRxiv a license to display the preprint in perpetuity. It is made available under aCC-BY 4.0 International license.

in 2020, stringent lineage-tracing strategies have revealed that neither quiescent nor reactive astrocytes convert to DANs upon PTBP1 depletion in the SNc or striatum (Chen et al., 2022; Hoang et al., 2023; Wang et al., 2021), fueling widespread debate about the origin of these *de novo* generated cells and their ability to alleviate motor deficits in PD mice (Arenas, 2020; Jiang et al., 2021; Qian et al., 2021).

In this study, we emplyed adenine base editors (ABEs), which enable gene editing independent of DNA double strand break formation (Gaudelli et al., 2017) and thus without the risk of inducing chromosomal rearrangements, translocations, or large deletions (Adikusuma et al., 2018; Kosicki et al., 2018; Shin et al., 2017), to install a loss-of-function splice mutation in the *Ptbp1* gene in astrocytes or neurons. Using a chemically-induced PD mouse model, we show that downregulation of neuronal rather than astroglial PTBP1 in the SNc and striatum improves forelimb akinesia and spontaneous rotations. Histological analysis revealed that downregulation of neuronal PTBP1 induced expression of tyrosine hydroxylase (TH), which is the rate-limiting enzyme in the biosynthesis of dopamine and other catecholamines and thus a characteristic marker of DANs, in non-dividing neurons of the striatum. Since lack or dysfunction of TH results in dopamine deficiency and parkinsonism, induction of TH expression in striatal neurons may explain the observed rescue of PD phenotypes in mice and provide therapeutic benefits for PD patients.

## Results

### Adenine base editing effectively downregulates PTBP1 in cell lines

Base editors (BEs) are CRISPR-Cas derived genome engineering tools that allow the precise conversion of A-T to G-C (adenine BEs, ABEs) or C-G to T-A (cytidine BEs, CBEs) base pairs in cell lines as well as post-mitotic cells (Gaudelli et al., 2017; Koblan et al., 2021; Komor et al., 2016; Levy et al., 2020; Villiger et al., 2018). BEs can thus be applied to precisely disrupt canonical splice sites and permanently eliminate gene function *in vivo* (Kluesner et al., 2021; Musunuru et al., 2021; Rothgangl et al., 2021; Winter et al., 2019). To achieve effective and permanent repression of PTBP1, we sought to utilize ABEs to mutate canonical splice sites. To assess if adenine base editing can be used to effectively disrupt PTBP1 expression, we designed seven sgRNAs targeting canonical *Ptbp1* splice donor or acceptor sites in murine Hepa1-6 cells (hereafter referred to as Hepa; Figure 1 – figure supplement 1). Plasmids expressing the sgRNAs were co-delivered with *Sp*Cas-, *Sp*G-, or *Sp*Cas-NG-ABE-expressing plasmids into Hepa cells, and genomic DNA was isolated at 5 days post-transfection for analysis by deep sequencing. In line with previous reports (Kluesner et al., 2021), base editing

bioRxiv preprint doi: https://doi.org/10.1101/2024.03.22.586274; this version posted October 8, 2024. The copyright holder for this preprint (which was not certified by peer review) is the author/funder, who has granted bioRxiv a license to display the preprint in perpetuity. It is made available under aCC-BY 4.0 International license.

activity was higher at splice donor sites, with the highest editing rates at the exon-intron junctions of exon 3 (92.9±1.0% for *Sp*G-ABE8e) and 7 (85.0±7.2% for *Sp*Cas-ABE8e; figure 1 – figure supplement 1). Next, we validated whether both sgRNAs resulted in a reduction of transcript and protein levels. Average editing rates of 77% (sgRNA-ex3) and 73% (sgRNA-ex7) on genomic DNA (Figure 1 – figure supplement 2) resulted in approximately 70% and 50% reduction of *Ptbp1* transcripts in Hepa cells (Figure 1 - figure supplement 2), leading to a substantial reduction in PTBP1 protein levels and a significant increase in the transcription of exons known to be repressed by PTBP1 (Han et al., 2014; Li et al., 2014) (Figure 1 - figure supplement 2).

To analyze whether PTBP1 can also be downregulated by adenine base editing in neuronal and astroglial cells, we repeated experiments with sgRNA-ex3 and the ABE8e-*Sp*G variant in the neuronal Neuro2a and astroglial C8-D1A cell lines (hereafter referred to as N2a and C8-D1A). Compared to Hepa cells (92.9±1.0%; figure 1 – figure supplement 2), editing rates were lower in both cell lines (N2a: 64±7.9%; C8-D1A: 62.7±15.1%; figure 1A). Nevertheless, we again detected a substantial reduction of *Ptbp1* mRNA and PTBP1 protein levels (Figure 1B and C). Notably, editing of the canonical splice donor at exon 3 generated alternative *Ptbp1* splice sites in all three cell lines (Figure 1 – figure supplement 3), which, however, did not result in functional PTBP1 protein (Figure 1C; figure 1 - figure supplement 2). Based on these results, we decided to use sgRNA-ex3 in combination with the *Sp*G-ABE8e variant for *in vivo* experiments.

**Downregulation of PTBP1 in neurons of the SNc generates TH-expressing cells**

To study the effect of PTBP1 downregulation on an injured nigrostriatal circuit in mice, we first induced a unilateral lesion in the medial forebrain bundle (mfb) using the toxic dopamine analogue 6-hydroxydopamine (6-OHDA; figure 2 – figure supplement 1) (da Conceição et al., 2010), similar to previous studies (Chen et al., 2022; Hoang et al., 2023; Qian et al., 2020; Zhou et al., 2020). 5 weeks after the introduction of a lesion, we quantified the loss of $TH^+$ DANs in the SNc and DA fibers in the striatum by histology (Figure 2 - figure supplement 1). As expected, 6-OHDA induced a severe unilateral lesion in the nigrostriatal pathway (Figure 2 – figure supplement 1), characterized by an average 99% reduction in the number of $TH^+$ DANs in the SNc ipsilateral to the injection site (intact hemisphere: 10547±2313 $TH^+$ cells; lesioned hemisphere: 114±83 $TH^+$ cells; figure 2 – figure supplement 1) and an average 92% decrease in fluorescence signal corresponding to striatal DA fibers (dorsal and ventral; figure 2 – figure supplement 1). In line with previous reports (Chen et al., 2022), we also observed a sharp

bioRxiv preprint doi: https://doi.org/10.1101/2024.03.22.586274; this version posted October 8, 2024. The copyright holder for this preprint (which was not certified by peer review) is the author/funder, who has granted bioRxiv a license to display the preprint in perpetuity. It is made available under aCC-BY 4.0 International license.

increase in activated astrocytes, as indicated by the upregulation of the intermediate filament protein GFAP (glial fibrillary acidic protein; figure 2 – figure supplement 1). Finally, we analyzed perturbations in spontaneous motor activities following the 6-OHDA lesion (Boix et al., 2015; Glajch et al., 2012; Iancu et al., 2005) and found that ipsilateral rotations and contralateral forelimb akinesia were significantly increased (Figure 2 – figure supplement 1).

In order to target PTBP1 in astrocytes or neurons of 6-OHDA-induced PD mice, we designed adeno-associated virus (AAV) vectors expressing the *Sp*G-ABE8e variant under the control of the astrocyte-specific short GFAP promoter (Lee et al., 2008) (hereafter referred to as AAV-GFAP), or the neuron-specific human synapsin 1 promoter (hsyn) (Kügler et al., 2003) (hereafter referred to as AAV-hsyn). Both vectors additionally express sgRNA-ex3 under the human U6 promoter (Duvoisin et al., 2012). As a non-targeting control, we generated an AAV vector that expresses *Sp*G-ABE8e from the ubiquitous Cbh promoter (Gray et al., 2011), but does not contain sgRNA-ex3 (hereafter referred to as AAV-ctrl). Since ABE8e exceeds the packaging capacity of a single AAV (~5 kb including ITRs) (Grieger and Samulski, 2005), we used the intein-mediated protein trans-splicing system from *Nostoc punctiforme* (*Npu*) (Li et al., 2008; Truong et al., 2015) to split the ABE for expression from two separate AAVs (Figure 2 – figure supplement 2). After confirming on-target editing in N2a and C8-D1A cells (Figure 2 – supplement 2), we packaged intein-split ABE8e expression vectors into AAV-PHP.eB capsids and delivered particles to the SNc of C57BL/6J mice 5 weeks after the introduction of the unilateral 6-OHDA lesion (Figure 2A). 12 weeks after AAV treatment at a dose of $2\times10^8$ vector genomes (vg) per animal, we assessed whether the injured nigrostriatal pathway was reconstituted (Figure 2A).

When we first analyzed animals treated with AAV-ctrl, we observed an average 99% reduction of $TH^+$ cells in the SNc of lesioned animals (intact hemisphere: 8678±2765 $TH^+$ cells; lesioned hemisphere: 122±26 $TH^+$ cells; Figure 2B and C). When we next assessed animals treated with AAV-hsyn to downregulate PTBP1 in neurons, we observed a restoration of approximately 10% of $TH^+$ cells compared to the intact hemisphere (intact hemisphere: 7613±1386 $TH^+$ cells; lesioned hemisphere: 721±144 $TH^+$ cells; Figure 2B and D). In contrast, when we analyzed animals treated with AAV-GFAP to downregulate PTBP1 in astrocytes, we did not observe $TH^+$ cells above control levels (intact hemisphere: 9209±1199 $TH^+$ cells; lesioned hemisphere: 158±78 $TH^+$ cells; figure 2C and D; figure 2 – figure supplement 3). However, despite the presence of TH+ cells in the SNc of AAV-hsyn-treated animals, we did not detect an increase in fluorescence signal corresponding to DA fibers in the striatum, suggesting that $TH^+$ cells generated in the SNc upon neuronal PTBP1 downregulation did not

bioRxiv preprint doi: https://doi.org/10.1101/2024.03.22.586274; this version posted October 8, 2024. The copyright holder for this preprint (which was not certified by peer review) is the author/funder, who has granted bioRxiv a license to display the preprint in perpetuity. It is made available under aCC-BY 4.0 International license.

form striatal projections (Figure 2E and F). Further supporting this observation, we did not detect differences in fluorescence intensity between groups when analyzing projections of DANs in the mfb (Figure 2 – figure supplement 4). Notably, base editing at the *Ptbp1* splice site (AAV-ctrl, 0.04±0.03%, AAV-GFAP, 14.7±3.9%; AAV-hsyn, 15.5±8.5%) as well as a reduction of *Ptbp1* transcript (AAV-GFAP, 23.7±12.7%; AAV-hsyn, 24.8±18.7%) and PTBP1 protein levels (AAV-GFAP, 10.8±6.3%; AAV-hsyn, 13.8±10.1%) could be confirmed in SNc tissues at experimental endpoints (Figure 2 – figure supplement 5).

Taken together, our results suggest that PTBP1 downregulation in neurons of the SNc generates $TH^+$ cells; however, unlike endogenous DANs in the SNc, they do not project to the dorsal striatum.

**Downregulation of PTBP1 in neurons of the striatum generates $TH^+$ cells and increases striatal dopamine levels**

Since the observed $TH^+$ cells in the SNc did not generate projections to reconstruct the nigrostriatal pathway, we next tested whether we could bypass the lack of striatal projections by generating $TH^+$ cells directly in the striatum. We therefore delivered AAV-hsyn at a dose of $4\times10^8$ vg per animal into the striatum of C57BL/6J mice, which were pre-treated with 6-OHDA to generate a unilateral lesion. The injection volume, and thus the delivered AAV dose, was increased compared to the SNc to achieve comparable AAV biodistribution in the larger striatum. Confirming the unilateral impairment of the nigrostriatal pathway, analysis of brain sections at 12 weeks post-treatment revealed an average 99% reduction of $TH^+$ cells in the lesioned SNc and no detectable DA projections to the striatum (Figure 3 – figure supplement 1). When we quantified $TH^+$ cells in brain sections of the striatum, we found 106±38 $TH^+$ cells across 3 sections (estimated as 2646±952 cells in the entire striatum) in mice treated with AAV-hsyn compared to no $TH^+$ cells in the lesioned hemisphere of animals treated with AAV-ctrl (Figure 3A). Analysis of striatum tissues isolated from AAV-ctrl- and AAV-hsyn-treated PD mice revealed base editing at the *Ptbp1* splice site (AAV-ctrl, 0.4±0.1%; AAV-hsyn, 23.0±6.6%; Figure 3 – figure supplement 2) and downregulation of *Ptbp1* transcript (AAV-hsyn, 30.8±14.6%) and PTBP1 protein levels (AAV-hsyn, 22.1±6.4%; figure 3 – supplement 2).

Since we did not observe PTBP1 downregulation or $TH^+$ cells in animals treated with AAV-ctrl (Figure 3A; figure 3 – figure supplement 2), we can rule out that TH expression is induced by 1) tissue damage due to the injection procedure or 2) toxicity due to the administered AAV dose or serotype. To additionally exclude that TH expression might be caused by off-target

bioRxiv preprint doi: https://doi.org/10.1101/2024.03.22.586274; this version posted October 8, 2024. The copyright holder for this preprint (which was not certified by peer review) is the author/funder, who has granted bioRxiv a license to display the preprint in perpetuity. It is made available under aCC-BY 4.0 International license.

editing effects, we experimentally determined off-target sites of sgRNA-ex3 using GUIDE-seq in N2a cells (Tsai et al., 2014) and subsequently analyzed these sites in treated animals by deep amplicon sequencing (Figure 3 – supplement 3). One off-target site was identified in the myopalladin (*Mypn*) gene, which encodes for a muscle-specific protein and plays a critical role in regulating the structure and growth of skeletal and cardiac muscle (Filomena et al., 2021, 2020), and another site was detected in the intronic region of the ankyrin-1 (*Ank1*) gene, which encodes for an adaptor protein linking membrane proteins to the underlying cytoskeleton (Cunha and Mohler, 2009). Importantly, base editing rates at both sites were substantially lower (*Mypn*, 5.4±1.7%; *Ank1*, 5.8±1.9%; Figure 3 – figure supplement 3) than at the *Ptbp1* site in AAV-hsyn-treated mice (23.0±6.6%; Figure 3 – figure supplement 2) and no reduction in transcript levels of the respective genes was observed (Figure 3 – figure supplement 3). Thus, the induction of TH expression upon adenine base editing with sgRNA-ex3 is likely a direct consequence of PTBP1 downregulation.

Next, we assessed whether the ectopic expression of TH in the striatum led to an increase in tissue dopamine levels. We manually dissected striata of lesioned and unlesioned hemispheres and quantified tissue dopamine levels by high-pressure liquid chromatography (HPLC; figure 3 – figure supplement 4). Peak identities and neurotransmitter concentrations were analyzed using corresponding standards of known concentrations. Importantly, base edited animals showed an approximately 2.5-fold increase in the concentration of striatal dopamine (AAV-hsyn: 4.4±2.6 nmol/g protein; AAV-ctrl: 1.7±0.7 nmol/g protein) and the dopamine metabolite 3,4-dihydroxyphenylacetic acid (DOPAC; AAV-hsyn: 8.2±3.9 nmol/g protein; AAV-ctrl: 3.1±1.8 nmol/g protein) in the lesioned hemisphere (figure 3 – figure supplement 4).

Taken together, our data suggest that downregulation of PTBP1 in striatal neurons of 6-OHDA-lesioned hemispheres resulted in the expression of TH and an elevation of striatal dopamine concentrations.

**Phenotypic characterization of TH$^+$ cells in the striatum**

To characterize the TH-expressing cells in the SNc and striatum of AAV-hsyn-treated mice in more detail, we co-stained them for the pan-neuronal marker NEUN (hexaribonucleotide binding protein-3). As expected, virtually all TH$^+$ cells in the intact SNc were co-stained for NEUN (99.0±0.1%; figure 3B). Likewise, the majority of TH$^+$ cells in the lesioned SNc (hsyn: 92.0±6.2%; figure 3B) and striatum of AAV-hsyn-treated animals (77.5±11.8%; figure 3C) were also labelled by NEUN, further corroborating a neuronal origin of these cells. Moreover, we observed a significant reduction in the surface area and Feret's diameter between

bioRxiv preprint doi: https://doi.org/10.1101/2024.03.22.586274; this version posted October 8, 2024. The copyright holder for this preprint (which was not certified by peer review) is the author/funder, who has granted bioRxiv a license to display the preprint in perpetuity. It is made available under aCC-BY 4.0 International license.

TH/NEUN double-positive cells in the lesioned striatum compared to endogenous DANs in the intact SNc, or TH/NEUN double-positive cell bodies in the lesioned SNc of AAV-hsyn-treated mice (Figure 3D).

Differences in the frequency of NEUN-labeling, as well as surface area and diameter of $TH^+$ cells in the striatum might be attributed to 1) varying maturation states of these cells, potentially influenced by the local microenvironment of the SNc vs striatum, and/or 2) TH-expressing cells originating from distinct neuronal subpopulations. In line with previous work (Qian et al., 2020), injection of AAV-hsyn into the visual cortex did not lead to TH expression in local neurons (Figure 3 – figure supplement 5; n=174 Cas9/NEUN double-positive cells), suggesting that the local microenvironment indeed plays a contributing role in inducing TH expression in the targeted neurons. To next analyze the origin of TH-expressing cells in the striatum, we first assessed whether these cells originated from dividing neural progenitors or mature, non-dividing neurons. We therefore supplied bromodeoxyuridine (BrdU)-containing drinking water to 6-OHDA-lesioned mice after AAV-hsyn treatment (Figure 3 – figure supplement 6). After confirming successful BrdU labeling of proliferating cells in the dentate gyrus (DG; figure 3 – figure supplement 6), we performed BrdU/NEUN/TH co-staining experiments with striatal sections. Microscopic analysis of 163 TH/NEUN double-positive cells revealed no co-labeling with BrdU (Figure 3 – figure supplement 6), indicating that $TH^+$ cells were not generated *de novo* and rather originated from non-proliferating mature neurons.

Next, we performed multiplexed iterative immunofluorescence imaging (4i) (Cole et al., 2022) on tissue sections to further characterize the identity, origin, and differentiation state of these cells (Figure 4). After successful validation of antibody specificities (Figure 4 – supplement 1), we performed four 4i rounds using markers for neural progenitors (SOX2/sex determining region Y-box 2, NES/neuroepithelial stem cell protein, DCX/doublecortin), DANs (TH, DAT), and mature neurons (NEUN, CTIP2/COUP-TF-interacting protein 2, SST/somatostatin, PV/parvalbumin, CALB2/calbindin 2). The majority of $TH^+$ cells also expressed the marker DAT (75.2±5.6%; figure 4A, B), further corroborating the DA identity of these cells. Moreover, supporting the results of our BrdU-labeling experiments (Figure 3 – figure supplement 6), only a small fraction of TH/DAT double-positive cells were labeled for markers of neural progenitors (SOX2, 9.1±2.4%; NESTIN, 2.1±0.5%; DCX, 2.6±0.8%; figure 4A, B). Instead, most TH/DAT-labeled cells expressed the adult pan-neuronal marker NEUN (86.2±3.7%; figure 4A, B). Of this TH/DAT/NEUN-positive population, 49.8±12.9% were additionally labeled with CTIP2 (Figure 4A and 4B), a marker for GABAergic medium spiny neurons (MSNs), and 46.4±10.4% expressed markers for various GABAergic interneurons

bioRxiv preprint doi: https://doi.org/10.1101/2024.03.22.586274; this version posted October 8, 2024. The copyright holder for this preprint (which was not certified by peer review) is the author/funder, who has granted bioRxiv a license to display the preprint in perpetuity. It is made available under aCC-BY 4.0 International license.

(PV, 3.2±1.9%; SST, 3.5±1.2%; CALB2, 39.7±11.0%; figure 4A and 4B), indicating that expression of DA markers may be achieved in various subtypes of GABAergic neurons upon PTBP1 downregulation.

In summary, our data show that TH-expressing cells were not generated from proliferating neural stem cells, but rather originated from various populations of post-mitotic striatal neurons that acquired DA characteristics upon PTBP1 downregulation.

**Neuronal PTBP1 repression alleviates drug-free motor dysfunction in PD mice**

Last, we evaluated whether neuronal and/or astroglial base editing of PTBP1 in the SNc and/or striatum could restore motor functions in mice with a unilateral 6-OHDA lesion. We first performed two common drug-free behavioral tests: the cylinder test to quantify the asymmetry of spontaneous rotations and the stepping test to quantify contralateral forelimb akinesia (Boix et al., 2015; Glajch et al., 2012; Iancu et al., 2005). We found that drug-free motor dysfunctions were significantly alleviated in animals treated with AAV-hsyn, but not with AAV-GFAP, in the SNc when using an AAV dose of $2\times10^8$ vg per animal (Figure 5 – figure supplement 1). Likewise, PTBP1 targeting in striatal neurons restored the asymmetry of spontaneous behaviors (Figure 5A and 5B). To assess the extent of motor improvements in response to the ABE treatment, we additionally tested two drug-induced motor behaviors. However, we did not detect recovery of contralateral rotations in treated animals after systemic administration of amphetamine (Figure 5C; figure 5 – figure supplement 1), which leads to an enhanced imbalance of extracellular dopamine concentrations between the denervated and intact striatum (Freyberg et al., 2016; Karam et al., 2022). Likewise, after systemic administration of apomorphine, which acts as a dopamine receptor agonist and stimulates hypersensitive dopamine receptors in the lesioned hemisphere (Arroyo-García et al., 2018; da Conceição et al., 2010; Iancu et al., 2005), we did not observe a recovery of ipsilateral rotations in any treatment group (Figure 5D; figure 5 – figure supplement 1).

Taken together, downregulation of PTBP1 in SNc and striatal neurons improves spontaneous, but not drug-induced, behaviors in 6-OHDA-lesioned mice.

**Discussion**

In this study, we applied adenine base editing to introduce *Ptbp1* loss-of-function mutations in astrocytes and neurons in the 6-OHDA-induced PD mouse model. Delivery of dual AAV vectors to the SNc resulted in the formation of TH-expressing cells and rescue of spontaneous behaviors when a neuronal promoter was used to drive ABE expression. However, no DA

bioRxiv preprint doi: https://doi.org/10.1101/2024.03.22.586274; this version posted October 8, 2024. The copyright holder for this preprint (which was not certified by peer review) is the author/funder, who has granted bioRxiv a license to display the preprint in perpetuity. It is made available under aCC-BY 4.0 International license.

projections to the striatum were detected, supporting recent findings that suggest a functional role of PTBP1 in promoting axon regeneration of adult sensory neurons (Alber et al., 2023). Reconstitution of the nigrostriatal pathway, which connects the SNc with the dorsal striatum (Kalia and Lang, 2015), is therefore unlikely the mechanism underlying the observed phenotypic rescue. Supporting this hypothesis, downregulation of neuronal PTBP1 in the striatum of 6-OHDA-lesioned mice also led to the formation of $TH^+$ cells and a rescue of spontaneous behaviors.

Two previous studies suggested that PTBP1 downregulation in the SNc, using either shRNA-mediated knockdown or knockdown via CRISPR-CasRx, led to the conversion of astrocytes into functional DANs in 6-OHDA-lesioned mice (Qian et al., 2020; Zhou et al., 2020). However, recent lineage tracing studies revealed that neither quiescent nor reactive astrocytes in the SNc or striatum convert to DANs upon PTBP1 downregulation (Chen et al., 2022; Hoang et al., 2023; Wang et al., 2021). Instead, these studies hypothesize that the reported effects might be attributed to leaky activation of the GFAP promoter in neurons, which could have been misinterpreted as astrocyte to neuron conversion. Our study contributes to this recently growing body of evidence, indicating that downregulation of astroglial PTBP1 does not induce astrocyte conversion into DANs, and that neurons are the origin of the observed $TH^+$ cells (Chen et al., 2022; Wang et al., 2021; Yang et al., 2023). Our 4i and BrdU experiments furthermore revealed that TH expression in the striatum was induced in mature neurons, either expressing markers of GABAergic MSNs or interneurons. These findings indicate that the induction of TH expression is not restricted to a specific neuronal subpopulation, but may rather be attributed to 1) potential bias of hsyn promoter activity towards inhibitory neurons (Radhiyanti et al., 2021), 2) preferential AAV tropism towards distinct neuronal subpopulations in the striatum, or 3) differences in the local microenvironment, chemical signals, and neuronal circuitry required to induce TH expression in distinct neuronal subpopulations.

While our study suggests that PTBP1 downregulation can enable TH expression in various GABAergic neuronal populations in the striatum, the transcriptional changes leading to and following TH expression in these cells remain unclear. Previous research has demonstrated that the interplay between microRNAs (miRNAs) and the RNA processing proteins PTBP1 and its homology nPTBP (PTBP2) is crucial during neuronal differentiation and maturation (Fig. 5 – figure supplement 2) (Boutz et al., 2007; Makeyev et al., 2007; Zheng et al., 2012). Key events in this signaling cascade are the dynamic release of PTBP1-mediated inhibition of miRNA-124,

bioRxiv preprint doi: https://doi.org/10.1101/2024.03.22.586274; this version posted October 8, 2024. The copyright holder for this preprint (which was not certified by peer review) is the author/funder, who has granted bioRxiv a license to display the preprint in perpetuity. It is made available under aCC-BY 4.0 International license.

which induces nPTBP expression and activates neuron-specific expression programs in non-neuronal cells (Makeyev et al., 2007; Xue et al., 2013). Thus, the activation of the PTBP1/nPTBP regulatory loops is essential for driving reprogramming towards the neuronal lineage and subsequent neuronal maturation (Xue et al., 2016, 2013). While this classical model of PTBP1 down-regulation and neuronal differentiation implies neglible expression or importance of PTBP1 in mature neurons, our results indicate that PTBP1 is sufficiently expressed and plays a functional role in mature neurons, with the installation of a loss-of-function mutation resulting in detectable reduction in relative protein amounts (Figure 2 – supplement 5; figure 3 – supplement 2) and behavioral improvements in a PD mouse model (Figure 5; figure 5 – supplement 1). Supporting these findings, a recent study demonstrated PTBP1 expression in axons of sensory and motor neurons as well as a functional role in sensation, injury response, and axonal regeneration (Alber et al., 2023). Further investigation using single cell transcriptional analysis of the PTBP1/nPTBP regulatory loops, pro-neuronal transcription factors (*Ascl1*, *Myt1l*, *Zic1*, *Brn2*, *NeuroD1*) (Xue et al., 2013), or transcription factors guiding the differentiation into DANs (*Nr4a2*, *LMx1a*, *LMx1b*, or *Pitx3* (Niu et al., 2021)) could provide insights into the transcriptional switches underlying TH expression in MSNs and interneurons as observed in our study.

MSNs, the principal neurons of the striatum (~95%), can be divided into two distinct subtypes based on their expression of dopamine receptors and their axonal projections (D1- or D2-MSNs) (Gerfen et al., 1990; Smith et al., 1998). Both the input to and output from D1- and D2-MSNs are dynamically controlled by striatal interneurons, which constitute approximately 5% of total striatal neurons (Clarke and Adermark, 2015). Since both MSNs and interneurons receive DA inputs from the SNc, their activity and excitability are strongly hampered when striatal dopamine is absent (Bamford et al., 2018; Gerfen and Surmeier, 2011; Kreitzer and Malenka, 2008). It therefore seems feasible that PTBP1 downregulation by adenine base editing and subsequent TH expression might have enabled local dopamine synthesis in the dorsal striatum, which may have been sufficient to partly restore the function of these cell populations and compensate for the depletion of DA inputs from the SNc. Supporting this hypothesis, a recent study has shown that depletion of the orphan G-protein coupled receptor 6 (GPR6) in D2-MSNs reduced intracellular cyclic adenosine monophosphate (cAMP) concentrations, leading to increased striatal dopamine and decreased involuntary movements following apomorphine treatment in 6-OHDA-lesioned PD mice (Sun et al., 2021). When we quantified dopamine levels in the striatum of AAV-hsyn-treated PD mice using HPLC, we observed a 2.5-fold increase in striatal dopamine, suggesting that induction of TH expression in striatal neurons

bioRxiv preprint doi: https://doi.org/10.1101/2024.03.22.586274; this version posted October 8, 2024. The copyright holder for this preprint (which was not certified by peer review) is the author/funder, who has granted bioRxiv a license to display the preprint in perpetuity. It is made available under aCC-BY 4.0 International license.

might establish a basal tone of extracellular dopamine despite the absence of striatal DA projections, akin to pharmacological replenishment in PD patients (Poewe et al., 2017). While the increase in dopamine levels was modest compared to 6-OHDA-lesioned rats treated with the dopamine precursor L-DOPA, which exhibited an increase in extracellular dopamine concentrations from ~0.04 fmol/µL to ~9-10 fmol/µL (Lindgren et al., 2010), our results indicate that even a modest increase in striatal dopamine is sufficient to rescue spontaneous motor behaviors in PD mice. This finding aligns with recent work showing that multiple unconditioned DA-dependent motor tasks can be sustained through a diffuse basal tone of extracellular dopamine in the striatum (Delignat-Lavaud et al., 2023). Conversely, basal dopamine levels were insufficient to improve amphetamine-induced behaviors in AAV-hsyn-treated PD mice in this study, potentially due to the lack of striatal projections from the SNc and/or insufficient availability of intracellular dopamine in striatal neurons. Likewise, the detected dopamine levels in striatal tissues were not sufficient to reverse the hypersensitivity of D1 and D2 receptors to the dopamine agonist apomorphine. Higher base editing rates, achievable using either single AAV delivery of smaller Cas9 orthologues or multiple injections into the rostral, medial, and caudal regions of the striatum, may result in more pronounced global PTBP1 downregulation and potentially higher tissue dopamine concentrations, leading to a broader behavioral rescue. Moreover, further analysis using fiber photometry or microdialysis could provide information on synaptic dopamine release and availability.

Transcriptional reprogramming is fundamental for neuronal differentiation and maturation, relying on various feedback and feed-forward circuits to regulate cell type-specific gene expression programs. While loss of PTBP1 is considered crucial for reducing neuronal apoptosis and inducing neuronal differentiation during development, its various roles in mature neurons during adulthood remains largely elusive. Further investigation using single cell transcriptional analysis or spatial transcriptomics is needed to identify the transcriptional changes driving the expression of DA markers in striatal GABAergic neurons upon PTBP1 downregulation. These experiments may also contribute to our understanding of how PTBP1 downregulation may affect cAMP metabolism, dopamine synthesis, and basal ganglia circuitry in PD mice. Finally, to fully explore the therapeutic potential of PTBP1 base editing, future studies should also combine detailed transcriptional analysis with stringent lineage-tracing technologies and *in vivo* assessment of synaptic dopamine availability and release in more sophisticated PD mouse models that exhibit neuropathological, motor, and cognitive aspects of the disease.

bioRxiv preprint doi: https://doi.org/10.1101/2024.03.22.586274; this version posted October 8, 2024. The copyright holder for this preprint (which was not certified by peer review) is the author/funder, who has granted bioRxiv a license to display the preprint in perpetuity. It is made available under aCC-BY 4.0 International license.

## Materials and methods

### Generation of plasmids

sgRNA plasmids were generated by ligating annealed and phosphorylated oligos into a BsmBI-digested lentiGuide-Puro (Addgene #52963) using T4 DNA ligase (NEB). To generate intein-split ABE plasmids for AAV production, inserts with homology overhangs were either ordered as gBlocks (IDT) or generated by PCR. Inserts were cloned into KpnI- and AgeI-digested AAV backbones using HiFi DNA Assembly Master Mix (NEB). All PCRs were performed using Q5 High-Fidelity DNA Polymerase (NEB). All plasmids were transformed into *Escherichia coli* Stable3 competent cells (NEB). The identity of all plasmids was confirmed by Sanger Sequencing. Primers used for cloning of all plasmids are listed in supplementary tables 1 and 2. LentiGuide-Puro was a gift from F. Zhang (Addgene plasmid nos. 52963).

### Cell culture transfection and genomic DNA preparation

Hepa1-6 (ATCC CRL-1830) cells were maintained in Dulbecco's modified Eagle's medium (DMEM) plus GlutaMAX (Thermo Fisher Scientific), supplemented with 10% (v/v) fetal bovine serum (FBS) and 1% penicillin/streptomycin (Thermo Fisher Scientific) at 37°C and 5% $CO_2$. Neuro2a (ATCC CCL-131) cells were maintained in Eagle's Minimum Essential Medium (EMEM), supplemented with 10% (v/v) FBS and 1% penicillin/streptomycin. C8-D1A [astrocyte type I clone, ATCC CRL-2541] were maintained in Dulbecco's modified Eagle's medium (DMEM) supplemented with 10% (v/v) fetal bovine serum (FBS) and 1% penicillin/streptomycin (Thermo Fisher Scientific) at 37°C and 5% $CO_2$. Cells were passaged every 3 to 4 days and maintained at confluency below 90%.

For the *in vitro* screening of sgRNA activities, cells were seeded in 96-well cell culture plates (Greiner) and transfected at 70% confluency using 0.5µl Lipofectamine™ 2000 (Thermo Fisher Scientific). If not stated otherwise, 300ng of BE and 100ng of sgRNA were used for transfections. Cells were incubated for 5 days after transfection and genomic DNA was isolated using a direct lysis as previously described (Böck et al., 2022). For analysis of transcript and protein levels, cells were seeded in a 48-well cell culture plate (Greiner) and transfected at 70% confluency using 1µl of Lipofectamine™ 2000 (Thermo Fisher Scientific). A small aliquot of the cells was used for isolation of genomic DNA by direct lysis as previously described (Böck et al., 2022). The remaining cells were split in half for RNA and protein isolation.

For the assessment of *in vivo* base editing performance, a 40 µm thick section of the SNc or striatum was used for manual dissection of these regions under a stereomicroscope. DNA was

bioRxiv preprint doi: https://doi.org/10.1101/2024.03.22.586274; this version posted October 8, 2024. The copyright holder for this preprint (which was not certified by peer review) is the author/funder, who has granted bioRxiv a license to display the preprint in perpetuity. It is made available under aCC-BY 4.0 International license.

subsequently isolated from tissue pieces by direct lysis as previously described (Böck et al., 2022).

RNA isolation and RT-qPCR

RNA was isolated from cultured cells or snap-frozen brain tissues (striatum or SNc) using the RNeasy Mini Kit (Qiagen) or the AllPrep DNA/RNA/Protein Mini Kit (Qiagen) according to the manufacturer's instructions. RNA (1000ng input) was subsequently reverse-transcribed to cDNA using random primers and the GoScript reverse transcriptase kit (Promega). RT-qPCR was performed using FIREPolymerase qPCR Master Mix (Solis BioDyne) and analyzed using a Lightcycler 480 system (Roche). Fold changes were calculated using the double ΔCt method. Primers used for RT-qPCR are listed in supplementary table 3.

Protein isolation and western blot

Protein was isolated from cultured cells or snap-frozen brain tissues (striatum or SNc) using radioimmunoprecipitation (RIPA) assay buffer (150 mM Tris pH 8.0, 150 mM NaCl, 0.1% SDS, 0.5% sodium deoxycholate, 1% NP-40; Thermo Fisher Scientific), supplemented with protease inhibitor cocktail (Roche), or the AllPrep DNA/RNA/Protein Mini Kit (Qiagen) according to the manufacturer's instructions. Protein concentrations of all samples were determined using the Pierce Bicinchoninic Acid (BCA) Protein Assay Kit (Thermo Fisher Scientific).

Equal amounts of protein (*in vitro* samples: 30 µg; *in vivo* samples: 40 µg) were separated by SDS-polyacrylamide gel electrophoresis (Thermo Fisher Scientific) and transferred to a 0.45-µm nitrocellulose membrane (Amersham). Membranes were incubated with rabbit anti-PTBP1 (1:10,000; cat. no. ab133734, Abcam) and mouse anti-actin beta (1:2,000; cat. no. ab8226; Abcam). Signals were detected by fluorescence using IRDye-conjugated secondary antibodies (LI-COR Biosciences) and a LICOR Odyssey ® DLx imaging system. Protein quantifications were performed in Fiji. All antibodies are listed in supplementary table 4.

Amplification for deep sequencing

PTBP1-specific oligos were used to generate targeted amplicons for deep sequencing. Input genomic DNA was first amplified in a 10µL reaction for 30 cycles using NEBNext High-Fidelity 2×PCR Master Mix (NEB). Amplicons were purified using AMPure XP beads (Beckman Coulter) and subsequently amplified for eight cycles using oligos with sequencing adapters. Approximately equal amounts of PCR products were pooled, gel purified, and

bioRxiv preprint doi: https://doi.org/10.1101/2024.03.22.586274; this version posted October 8, 2024. The copyright holder for this preprint (which was not certified by peer review) is the author/funder, who has granted bioRxiv a license to display the preprint in perpetuity. It is made available under aCC-BY 4.0 International license.

quantified using a Qubit 3.0 fluorometer and the dsDNA HS Assay Kit (Thermo Fisher Scientific). Paired-end sequencing of purified libraries was performed on an Illumina Miseq platform. Oligos for deep sequencing are listed in supplementary table 5.

HTS data analysis

Sequencing reads were first demultiplexed using the Miseq Reporter (Illumina). Next, amplicon sequences were aligned to their reference sequences using CRISPResso2 (Clement et al., 2019). Adenine base editing efficiencies at splice sites were calculated as percentage of (number of reads containing edits at splice site)/(number of total aligned reads). Reference nucleotide sequences are listed in supplementary table 6.

GUIDE-seq off-target analysis

Briefly, $6\times10^4$ N2a cells were plated in a 24-well plate one day prior to transfection. Cells were transfected using Lipofectamine 3000 according to the manufacturer's instructions. Three plasmids, encoding for the *Sp*G Cas9 nuclease [333 ng], the *Ptbp1* sgRNA-3 [167 ng], and GFP [6 ng], were co-transfected with 12 pmol of the double-stranded oligodeoxynucleotide (dsODN) following the the original GUIDE-seq protocol (Tsai et al., 2014). Transfections were performed in triplicates. dsODN was transfected as a negative control. Cells were harvested ~96 h post-transfection and genomic DNA was purified. Efficient indel formation at the on-target site and integration of the dsODN tag were confirmed through deep amplicon sequencing. Genomic DNA was subsequently sheared with Covaris E220 to on average 500 bp according to the manufacturer's protocol. Sample libraries were assembled as previously described (Tsai et al., 2014) and sequenced using the Illumina MiSeq platform. Data were analysed using open-source guideseq software (version 1.1) (Tsai et al., 2016). Consolidated reads were mapped to the mouse mm39 reference genome. Upon identification of the genomic regions integrating the dsODNs in the aligned data, off-target sites with maximum six mismatches to the on-target site, which were absent in the background controls, were retained. A summary of the GUIDE-seq results can be found in Supplementary File 1.

AAV production

Pseudo-typed vectors (AAV2 serotype PHP.eB) were produced by the Viral Vector Facility of the Neuroscience Center Zurich. Briefly, AAV vectors were ultracentrifuged and diafiltered. Physical titers (vector genomes per milliliter, vg/mL) were determined using a Qubit 3.0

bioRxiv preprint doi: https://doi.org/10.1101/2024.03.22.586274; this version posted October 8, 2024. The copyright holder for this preprint (which was not certified by peer review) is the author/funder, who has granted bioRxiv a license to display the preprint in perpetuity. It is made available under aCC-BY 4.0 International license.

fluorometer (Thermo Fisher Scientific) as previously published (Düring et al., 2020). The identity of the packaged genomes of each AAV vector was confirmed by Sanger sequencing.

Animal studies

Animal experiments were performed in accordance with protocols approved by the Kantonales Veterinäramt Zürich and in compliance with all relevant ethical regulations. C57BL/6J mice were housed in a pathogen-free animal facility at the Institute of Pharmacology and Toxicology of the University of Zurich. Mice were kept in a temperature- and humidity-controlled room on a 12-hour light-dark cycle. Mice were fed a standard laboratory chow (Kliba Nafag no. 3437 with 18.5% crude protein) with ad libitum access to food and water. Exclusion criteria were pre-defined during study design to meet ethical regulations. No animal was excluded from the study.

Stereotactic injections in mice

Unless stated otherwise, adult female C57BL/6J mice at P50-P60 were used to introduce a unilateral lesion in the medial forebrain bundle. Buprenorphine [0.1 mg/kg bodyweight], was administered to mice subcutaneously 30 min prior to surgery. Animals were anesthetized using isoflurane (5% isoflurane with 1000 mL/min in 100% $O_2$) and placed into a stereotaxic mouse frame on a warming surface to maintain body temperature. Anesthesia was maintained at 1.5-2.5% isoflurane with 400 mL/min in 100% $O_2$ during surgeries. Mice were pre-treated with desipramine [25 mg/kg bodyweight] and pargyline [5 mg/kg bodyweight] 30 min before the injection of 6-hydroxydopamine (6-OHDA) was performed. 6-OHDA was dissolved in 0.02% ascorbate/saline solution at a concentration of 15 mg/mL and used within a maximum of 3h. 3.6µg of 6-OHDA were injected into the medial forebrain bundle (mfb) at the following coordinates (relative to bregma): -1.2 mm anteroposterior (AP); 1.3 mm mediolateral (ML); -5 mm dorsoventral (DV). Sham-injected mice were injected with 0.02% ascorbate/saline solution. Injections were performed using a 5µL Hamilton syringe with a 33G needle at a speed of 0.05 µL/min. The needle was slowly removed 3min after the injection and the wound was sutured using Vicryl 5-0 suture (Ethicon). Animals with unilateral lesions received extensive post-operative care for two weeks. After the lesion, animals received daily glucose injections, and kitten milk (Royal Canin) for one week to support recovery.

4-5 weeks after the introduction of the 6-OHDA lesion, AAVs were injected into the substantia nigra, striatum, or visual cortex at the following coordinates (relative to bregma): -3.0 mm anteroposterior (A/P), 1.2 mm mediolateral (M/L), -4.5 mm dorsoventral (D/V) for

bioRxiv preprint doi: https://doi.org/10.1101/2024.03.22.586274; this version posted October 8, 2024. The copyright holder for this preprint (which was not certified by peer review) is the author/funder, who has granted bioRxiv a license to display the preprint in perpetuity. It is made available under aCC-BY 4.0 International license.

the substantia nigra pars compacta; 0.38 mm A/P, 1.8 mm M/L, -4:0.4:-2.4 mm D/V for the striatum; and -4.5 mm A/P, 2.7 mm ML, 0.35 mm D/V for the visual cortex. Injections were performed using the same size needle, syringe, and speed as before. The needle was slowly removed 3min after the injection and the wound was sutured using Vicryl 5-0 suture (Ethicon).

Behavioral assays

Behavior experiments were performed at 4 weeks after the 6-OHDA lesion and 12 weeks after delivery of the treatment. Scientists performing and analyzing behavioral data were blinded during the study. To analyze spontaneous rotations during the dark phase of the light cycle, mice were individually placed into a glass cylinder (10cm diameter, 14cm height) and after 1min of habituation mouse behavior was recorded from the bottom using a digital camera. For assessment of spontaneous rotations after treatment, animals were first habituated to the experimental environment on three separate days. Full body ipsi- and contralateral turns (360°) were counted for 10min. A frame-by-frame video player (VLC media player) was used for scoring. Data are expressed as a percentage of ipsilateral rotations from total rotations.

To assess forelimb akinesia during the light phase of the light cycle, we quantified left and right forelimb usage in the stepping test (Blume et al., 2009; Olsson et al., 1995). First, the animal was allowed to settle at one edge of the table (~2s) with all limbs on the table. Next, the experimenter lifted the hind legs of the mouse by pulling up the tail, leaving only the forepaws touching the table. Animals were pulled backwards by the tail at a steady pace of approximately 1m in 3-4s for a total distance of 1m. Two trials of three consecutive repetitions were performed per animal with at least 10min break between the two trials. Behavior was recorded from the side using a digital camera and the number of adjusting steps from both forepaws was counted. Data are represented as percentage of ipsilateral steps from total steps.

For assessing drug-induced rotations, D-amphetamine (5 mg/kg bodyweight; Sigma-Aldrich) or apomorphine (0.5 mg/kg bodyweight; Sigma-Aldrich) was administered to mice via intraperitoneal injections. Following the injection, mice were placed in a recovery cage for 10min. Afterwards, mice were placed in a cylinder (10cm diameter, 15cm height) and habituated for 1min. Rotations induced by D-amphetamine or apomorphine were recorded from the bottom for 10min using a digital camera and only fully-body turns (360°) were counted as previously described. Data are expressed as percentage of ipsilateral or contralateral rotations from total rotations.

Trans-cardiac perfusion, brain isolation, and dissection of brain regions

bioRxiv preprint doi: https://doi.org/10.1101/2024.03.22.586274; this version posted October 8, 2024. The copyright holder for this preprint (which was not certified by peer review) is the author/funder, who has granted bioRxiv a license to display the preprint in perpetuity. It is made available under aCC-BY 4.0 International license.

Sodium pentobarbital (Kantonsapotheke Zürich) was injected via intraperitoneal injection at a dose of 100mg/kg. Complete anesthesia was confirmed by the absence of a toe pinch reflex. Mice were placed on a perfusion stage inside a collection pan and the peritoneal cavity was exposed. The diaphragm was cut through laterally and the rib cage was cut parallel to the lungs, creating a chest "flap". The flap was clamped in place using a hemostat (Fine Science Tools) and a 25G needle (Sterican), attached to silicon tubing and a peristaltic pump, was inserted into the left ventricle. The right atrium was cut for drainage. Animals were first perfused with ice-cold PBS (Thermo Fisher Scientific) at a rate of 10mL/min, followed by perfusion with ice-cold fixative at the same rate (4% paraformaldehyde, PFA, Sigma-Aldrich). Once the perfusion was complete, mice were decapitated and the skull was removed with scissors and tweezers without inflicting damage to the underlying tissue. The brain was removed using a spatula.

For histology, PFA-perfused brains were post-fixated in 4% PFA for 4h, followed by overnight incubation in 30% sucrose. For neurotransmitter quantifications, brains were isolated, rinsed in PBS, and cut into 1mm slices using an acrylic mouse brain matrix (AgnThos) and razor blades. The striatum was isolated under a stereomicroscope using the mouse brain atlas (Paxinos and Franklin, 2001). For amplicon sequencing, regions of interest (striatum or SNc) were manually dissected from 40µm-thick coronal sections under a stereomicroscope using the mouse brain atlas (Paxinos and Franklin, 2001).

Immunohistochemistry

Fresh or snap-frozen PFA-fixed brain tissues of C57BL/6J mice were cut into 40µm-thick sections using a microtome. Sections were blocked in PBS supplemented with 5% normal donkey serum (cat. no. ab7475, abcam) and 0.3% Triton X-100 (Sigma-Aldrich) for 1h. Brain sections were incubated with primary antibodies overnight at 4°C (rabbit-NEUN, 1:1'000, abcam 177487; mouse-TH; 1:1'000, Immunostar 22941; chicken-GFAP, 1:1'500, abcam ab95231; rat-BrdU, 1:400, Oxford Biotech OBT0030). Donkey anti-rabbit-488 (1:1'000), donkey anti-mouse-594 (1:500), donkey anti-chicken-647 (1:500) and donkey anti-rat-647 (1:500; all from Jackson ImmunoResearch) were used as secondary antibodies and sections were counterstained with 4′,6-diamidino-2-phenylindole (DAPI, Sigma-Aldrich). Mounting was performed using Prolong Gold Antifade Mountant (Thermo Fisher Scientific). Images were taken with a Zeiss LSM 900 or a Zeiss AxioScan.Z1 slidescanner and analyzed with Fiji (Schindelin et al., 2012) or cell profiler (Stirling et al., 2021). The numerical density of cells was estimated using optical dissection (NvVref method). Density of striatal fibres in the lesioned hemisphere was quantified as relative fluorescence intensity (FI) compared to the

bioRxiv preprint doi: https://doi.org/10.1101/2024.03.22.586274; this version posted October 8, 2024. The copyright holder for this preprint (which was not certified by peer review) is the author/funder, who has granted bioRxiv a license to display the preprint in perpetuity. It is made available under aCC-BY 4.0 International license.

612 intact hemisphere. Additionally, the FI of the TH staining detected in the corpus callosum of
613 each hemisphere was used for background correction of the FI detected in the striatum of the
614 same hemisphere. Antibodies are listed in supplementary table 4.
615
616 Iterative immunofluorescence imaging (4i) and image analysis
617 Frozen PFA-fixed brain tissues of C57BL/6J mice were cut into 40µm-thick sections using a
618 microtome. Before mounting the sections, glass-bottomed 24-well plates (Cellvis P24-1.5H-
619 N) were coated with poly-D-lysine (0.1mg/mL, Sigma-Aldrich) for 5min at RT on a shaker.
620 Afterwards, wells were rinsed three times with deionized water and left to dry overnight. Tissue
621 sections were washed three times in PBS and transferred into the coated wells containing
622 500µL of PBS, which was carefully aspirated with a glass pipette to allow the sections to adhere
623 flat to the bottom. Sections were left to dry until there was no visible liquid remaining around
624 the edges of the sections. Next, tissue sections were rinsed with PBS (3×5min), followed by 1h
625 incubation in blocking solution (PBS supplemented with 3% donkey serum, 0.5% Triton X-
626 100, and 0.025% PFA) at RT. Sections were then incubated in primary antibodies (list in
627 supplementary table 4), diluted in blocking solution, for 3 nights at 4°C. Next, sections were
628 washed in PBS (3×5min), rinsed in blocking solution for 5min, followed by incubation with
629 secondary antibodies and DAPI (1:1000; stock 1mg/mL) for 2h at RT. All following steps were
630 performed under low light conditions to reduce possible fluorophore crosslinking. Last,
631 sections were washed in PBS (3×5min) and imaging buffer (PBS supplemented with N-Acetyl-
632 cysteine at 0.7M final concentration, pH 7.4) was added at least 5min prior to imaging to
633 guarantee penetrance of tissue sections. Once the imaging cycle had finished, sections were
634 rinsed three times with $dH_20$ and incubated in equal amounts of $dH_20$ and elution buffer
635 (3×5min; 0.5M L-glycine, 3M urea, 3M guanidine hydrochloride, 0.07M TCEP-HCl; pH 2.5).
636 Successful elution of each antibody was visually confirmed using a fluoresence microscope.
637 After elution, tissue sections were washed three times in PBS (5min) and then another 4i round
638 was started. A total of 4 imaging cycles were performed.
639 All 4i z-stacks (image intervals of 0.5µm) were collected on an ImageXpress Confocal HT
640 confocal laser-scanning microscope with a 20x water objective (NA 0.95) using bi-directional
641 scanning. Samples of the same imaging cycle were labeled with the same antibodies and images
642 were collected with identical microscopy settings for laser power, gain, digital offset, pinhole
643 diameter, and z-step. Images from tile scans were exported using MetaXpress and analyzed
644 using Fiji (Schindelin et al., 2012). DAPI intensity patterns were used to align image tiles from
645 different staining cycles.

bioRxiv preprint doi: https://doi.org/10.1101/2024.03.22.586274; this version posted October 8, 2024. The copyright holder for this preprint (which was not certified by peer review) is the author/funder, who has granted bioRxiv a license to display the preprint in perpetuity. It is made available under aCC-BY 4.0 International license.

646

647 *In vivo* BrdU proliferation assay

648 Five days after delivery of the treatment, bromodeoxyuridine was administered to mice at a
649 concentration of 0.8 mg/mL via drinking water. Frozen PFA-fixed brain tissues of BrdU-
650 treated mice were cut into 40µm-thick sections using a microtome. Sections were washed
651 2×15min and 1×5min in PBS, followed by a 10min incubation in 1M HCl on ice, and a 25min
652 incubation in 2M HCl at 37°C. Next, tissues were rinsed in 0.1M borate buffer (Sigma-Aldrich)
653 for 10min on a shaker at RT. After the tissues were rinsed in PBS for 6×10min, brain tissues
654 were stained as described in section "Immunohistochemistry".

655

656 Neurotransmitter purification and UHPLC-ECD quantifications

657 Snap-frozen fresh striata of lesioned or unlesioned hemispheres were used for the purification
658 of neurotransmitters. All materials were kept cold on dry ice during the whole purification
659 procedure and samples were kept under low light conditions on ice. Tissue samples were
660 powderized with 2 pulses (at maximum intensity) using a CryoPrepTM system (Covaris).
661 Equal amounts of powder were transferred to a pre-cooled 2 mL tube. For homogenization of
662 the tissue powder, a metal ball (Qiagen) and 1mL homogenization buffer (100mM Tris-HCl,
663 2mM EDTA, pH 7.6 supplemented with protease inhibitor tablet) were added to each tube and
664 samples were homogenized for 2×90s at 20 Hz using a TissueLyser II (Qiagen). Next, samples
665 were centrifuged for 20min at maximum speed and 4°C. Lysates were next transferred to fresh
666 pre-cooled tubes and 1M HCl was added to a final concentration of 10% (v/v). Subsequently,
667 lysates were filtered using an Amicon Ultra 0.5 (Sigma-Aldrich) and a table top centrifuge
668 (30min at 4°C and maximum speed). 20µL of the filtered sample was used for quantification
669 of total protein amounts. Protein concentrations were determined using the ABBOT Alinity C
670 System (Abbot, Abbotpark, Illinois, USA, kit-no. 7P5920). 20µL of the filtered sample was
671 used in parallel for quantification of neurotransmitter levels by UHPLC-ECD. Brain
672 monoamine neurotransmitter metabolites were analyzed in the filtered lysate using a modified
673 Thermo Fisher UltiMate 3000 High Sensitivity HPLC Electrochemical System (Thermo Fisher
674 Scientific, Waltham, Massachusetts, USA). Injection volume of each sample was 20 µL and
675 separation of the compounds was achieved using an YMC-Hydrosphere UHPLC column (C18
676 12 nm, S-2.0 µm, 150 x 30 mm, YMC Inc., Wilmington, NC, USA). As a mobile phase, a
677 56.7mM sodium phosphate buffer, containing 5mM octanesulphonic acid, 50µM EDTA,
678 0.28% phosphoric acid (85%), and 23% methanol (pH 2.9-3.1, adjust with concentrated 10M
679 NaOH), was used with an isocratic flow rate of 410 µL/min. The column was maintained at

bioRxiv preprint doi: https://doi.org/10.1101/2024.03.22.586274; this version posted October 8, 2024. The copyright holder for this preprint (which was not certified by peer review) is the author/funder, who has granted bioRxiv a license to display the preprint in perpetuity. It is made available under aCC-BY 4.0 International license.

27°C by a surrounding TCC-3000SD column-thermostat. The analytical cell (Coulometric Cell Model 6011RS, Thermo Fisher Scientific) within the electrochemical detector ECD-3000RS (Thermo Fisher Scientific) was adjusted to a 10mV potential and 100µA gain range for the upstream electrode, plus 400mV potential, plus 500nA gain range for the downstream electrode with a response time of 1s. Data was analyzed using the Chromeleon Chromatography Data System (CDS) Software 7.1.9 (Thermo Fisher) and corrected for the protein concentrations of the respective homogenates. All measurements were performed at the clinical chemistry unit of the Kinderspital Zürich.

Statistical analysis

All statistical analyses were performed using GraphPad Prism 10.2.0 for macOS. If not stated otherwise, data are represented as biological replicates and are depicted as means±standard deviation (s.d.). The sample size was approximated based on so-called Fermi methods and experience from previous base editing studies during experimental design. Sample sizes and the statistical analyses performed are described in the respective figure legends. Data were tested for normality using the Shapiro-Wilk test if not stated otherwise. For all analyses, a *P*-value of $P<0.05$ was considered statistically significant.

**Acknowledgements**

We thank the Functional Genomics Center Zurich (FGCZ) for technical support and access to instruments at the University of Zurich. We thank Cornelia Schwerdel for technical support during *in vitro* and staining experiments. Annina Denoth Lipuner and Sebastian Jessberger are acknowledged for help with planning and setting up 4i experiments and sharing antibodies. Members of the Schwank, Patriarchi, and Häberle labs are acknowledged for discussions and comments on the manuscript.

**Funding information**

This work was supported by the Swiss National Science Foundation (SNSF) grant no. 310030_185293 (to G.S.) and 310030_196455 (to T.P.), Novartis Foundation for Medical-Biological Research no. FN20-0000000203 (to D.B.), SNSF Spark fellowship no. 196287 (to D.B.), the URPP Itinerare (to G.S. and to D.B.), the Helmut Horten Foundation (to G.S.), and the European Research Council (ERC) under the European Union's Horizon 2020 research and innovation program (grant agreement: 891959; to T.P.).

bioRxiv preprint doi: https://doi.org/10.1101/2024.03.22.586274; this version posted October 8, 2024. The copyright holder for this preprint (which was not certified by peer review) is the author/funder, who has granted bioRxiv a license to display the preprint in perpetuity. It is made available under aCC-BY 4.0 International license.

## Author contributions

Conceptualization: D.B. and M.W.; Methodology: D.B. and M.W.; Investigation and Validation: D.B., M.W., J.M., D.F.C., P.I.K., S.A.; Visualization: D.B. and P.I.K.; Formal analysis: D.B., M.W., J.M., D.F.C., P.I.K., S.A., A.C., A.R., J.H., T.P., and G.S.; Resources and Data curation: T.P. and G.S.; Writing – original draft: D.B.; Writing – review&editing: D.B., M.W., J.M., D.F.C, P.I.K., S.A., A.C., A.R., J.H., T.P., and G.S.; Supervision and project administration: D.B. and M.W.; Funding acquisition: D.B., T.P., and G.S..

## Data availability

All data associated with this study are present in the paper. Illumina sequencing data is available under accession number GSE237570 at the Gene Expression Omnibus (GEO) and bioproject number PRJNA1155634 at the NCBI Sequence Read Archive.

## Competing interest declaration

G.S. is an advisor to Prime Medicine.

## Correspondence

Correspondence should be addressed to Tommaso Patriarchi (patriarchi@pharma.uzh.ch), Gerald Schwank (schwank@pharma.uzh.ch), or Desiree Böck (desiree.boeck@uzh.ch).

## References

Adikusuma F, Piltz S, Corbett MA, Turvey M, McColl SR, Helbig KJ, Beard MR, Hughes J, Pomerantz RT, Thomas PQ. 2018. Large deletions induced by Cas9 cleavage. *Nature*. doi:10.1038/s41586-018-0380-z

Alber S, Di Matteo P, Zdradzinski MD, Costa ID, Medzihradszky KF, Kawaguchi R, Di Pizio A, Freund P, Panayotis N, Marvaldi L, Doron-Mandel E, Okladnikov N, Rishal I, Nevo R, Coppola G, Joon Lee S, Sahoo PK, Burlingame AL, Twiss JL, Fainzilber M. 2023. PTBP1 regulates injury responses and sensory pathways in adult peripheral neurons. *Sci Adv* **9**. doi:10.1126/SCIADV.ADI0286/SUPPL_FILE/SCIADV.ADI0286_DATA_S1_AND_S2.ZIP

Arenas E. 2020. Method to combat Parkinson's disease by astrocyte-to-neuron conversion. *Nat 2021 5827813* **582**:489–490. doi:10.1038/d41586-020-01817-4

Arroyo-García LE, Vázquez-Roque RA, Díaz A, Treviño S, De La Cruz F, Flores G,

bioRxiv preprint doi: https://doi.org/10.1101/2024.03.22.586274; this version posted October 8, 2024. The copyright holder for this preprint (which was not certified by peer review) is the author/funder, who has granted bioRxiv a license to display the preprint in perpetuity. It is made available under aCC-BY 4.0 International license.

748 Rodríguez-Moreno A. 2018. The Effects of Non-selective Dopamine Receptor
749 Activation by Apomorphine in the Mouse Hippocampus. *Mol Neurobiol* **55**.
750 doi:10.1007/s12035-018-0991-2
751 Bamford NS, Wightman RM, Sulzer D. 2018. Dopamine's Effects on Corticostriatal
752 Synapses during Reward-Based Behaviors. *Neuron* **97**:494–510.
753 doi:10.1016/J.NEURON.2018.01.006
754 Bloem BR, Okun MS, Klein C. 2021. Parkinson's disease. *Lancet* **397**:2284–2303.
755 doi:10.1016/S0140-6736(21)00218-X
756 Blume SR, Cass DK, Tseng KY. 2009. Stepping test in mice: A reliable approach in
757 determining forelimb akinesia in MPTP-induced Parkinsonism. *Exp Neurol* **219**.
758 doi:10.1016/j.expneurol.2009.05.017
759 Böck D, Rothgangl T, Villiger L, Schmidheini L, Matsushita M, Mathis N, Ioannidi E,
760 Rimann N, Grisch-Chan HM, Kreutzer S, Kontarakis Z, Kopf M, Thöny B, Schwank G.
761 2022. In vivo prime editing of a metabolic liver disease in mice. *Sci Transl Med* **14**.
762 doi:10.1126/scitranslmed.abl9238
763 Boix J, Padel T, Paul G. 2015. A partial lesion model of Parkinson's disease in mice -
764 Characterization of a 6-OHDA-induced medial forebrain bundle lesion. *Behav Brain Res*
765 **284**. doi:10.1016/j.bbr.2015.01.053
766 Boutz PL, Stoilov P, Li Q, Lin CH, Chawla G, Ostrow K, Shiue L, Ares M, Black DL. 2007.
767 A post-transcriptional regulatory switch in polypyrimidine tract-binding proteins
768 reprograms alternative splicing in developing neurons. *Genes Dev* **21**:1636–1652.
769 doi:10.1101/GAD.1558107
770 Brown RC, Lockwood AH, Sonawane BR. 2005. Neurodegenerative diseases: An overview
771 of environmental risk factors. *Environ Health Perspect*. doi:10.1289/ehp.7567
772 Buffo A, Rite I, Tripathi P, Lepier A, Colak D, Horn AP, Mori T, Götz M. 2008. Origin and
773 progeny of reactive gliosis: A source of multipotent cells in the injured brain. *Proc Natl*
774 *Acad Sci U S A* **105**. doi:10.1073/pnas.0709002105
775 Chen W, Zhen Q, Huang Q, Ma S, Li M. 2022. Repressing PTBP1 fails to convert reactive
776 astrocytes to dopaminergic neurons in a 6-hydroxydopamine mouse model of
777 Parkinson's disease. *Elife* **11**. doi:10.7554/ELIFE.75636
778 Clement K, Rees H, Canver MC, Gehrke JM, Farouni R, Hsu JY, Cole MA, Liu DR, Joung
779 JK, Bauer DE, Pinello L. 2019. CRISPResso2 provides accurate and rapid genome
780 editing sequence analysis. *Nat Biotechnol*. doi:10.1038/s41587-019-0032-3
781 Cohen DE, Melton D. 2011. Turning straw into gold: Directing cell fate for regenerative

bioRxiv preprint doi: https://doi.org/10.1101/2024.03.22.586274; this version posted October 8, 2024. The copyright holder for this preprint (which was not certified by peer review) is the author/funder, who has granted bioRxiv a license to display the preprint in perpetuity. It is made available under aCC-BY 4.0 International license.

782 medicine. *Nat Rev Genet*. doi:10.1038/nrg2938
783 Cole JD, Del Castillo JS, Gut G, Gonzalez-Bohorquez D, Pelkmans L, Jessberger S. 2022.
784 Characterization of the neurogenic niche in the aging dentate gyrus using iterative
785 immunofluorescence imaging. *Elife* **11**. doi:10.7554/ELIFE.68000
786 Cunha SR, Mohler PJ. 2009. Ankyrin protein networks in membrane formation and
787 stabilization. *J Cell Mol Med* **13**:4364. doi:10.1111/J.1582-4934.2009.00943.X
788 da Conceição FSL, Ngo-Abdalla S, Houzel JC, Rehen SK. 2010. Murine model for
789 Parkinson's disease: From 6-OH dopamine lesion to behavioral test. *J Vis Exp*.
790 doi:10.3791/1376
791 de Lau LM, Breteler MM. 2006. Epidemiology of Parkinson's disease. *Lancet Neurol*.
792 doi:10.1016/S1474-4422(06)70471-9
793 Delignat-Lavaud B, Kano J, Ducrot C, Massé I, Mukherjee S, Giguère N, Moquin L,
794 Lévesque C, Burke S, Denis R, Bourque MJ, Tchung A, Rosa-Neto P, Lévesque D, De
795 Beaumont L, Trudeau LÉ. 2023. Synaptotagmin-1-dependent phasic axonal dopamine
796 release is dispensable for basic motor behaviors in mice. *Nat Commun 2023 141* **14**:1–
797 24. doi:10.1038/s41467-023-39805-7
798 Düring DN, Dittrich F, Rocha MD, Tachibana RO, Mori C, Okanoya K, Boehringer R, Ehret
799 B, Grewe BF, Gerber S, Ma S, Rauch M, Paterna JC, Kasper R, Gahr M, Hahnloser
800 RHR. 2020. Fast Retrograde Access to Projection Neuron Circuits Underlying Vocal
801 Learning in Songbirds. *Cell Rep* **33**. doi:10.1016/j.celrep.2020.108364
802 Duvoisin R, Ayuk MA, Rinaldi G, Suttiprapa S, Mann VH, Lee CM, Harris N, Brindley PJ.
803 2012. Human U6 promoter drives stronger shRNA activity than its schistosome
804 orthologue in Schistosoma mansoni and human fibrosarcoma cells. *Transgenic Res* **21**.
805 doi:10.1007/s11248-011-9548-0
806 Elbaz A, Dufouil C, Alpérovitch A. 2007. Interaction between genes and environment in
807 neurodegenerative diseases. *Comptes Rendus - Biol*. doi:10.1016/j.crvi.2007.02.018
808 Filomena MC, Yamamoto DL, Caremani M, Kadarla VK, Mastrototaro G, Serio S,
809 Vydyanath A, Mutarelli M, Garofalo A, Pertici I, Knöll R, Nigro V, Luther PK, Lieber
810 RL, Beck MR, Linari M, Bang ML. 2020. Myopalladin promotes muscle growth
811 through modulation of the serum response factor pathway. *J Cachexia Sarcopenia*
812 *Muscle* **11**:169. doi:10.1002/JCSM.12486
813 Filomena MC, Yamamoto DL, Carullo P, Medvedev R, Ghisleni A, Piroddi N, Scellini B,
814 Crispino R, D'autilia F, Zhang J, Felicetta A, Nemska S, Serio S, Tesi C, Catalucci D,
815 Linke WA, Polishchuk R, Poggesi C, Gautel M, Bang ML. 2021. Myopalladin knockout

bioRxiv preprint doi: https://doi.org/10.1101/2024.03.22.586274; this version posted October 8, 2024. The copyright holder for this preprint (which was not certified by peer review) is the author/funder, who has granted bioRxiv a license to display the preprint in perpetuity. It is made available under aCC-BY 4.0 International license.

816 mice develop cardiac dilation and show a maladaptive response to mechanical pressure
817 overload. *Elife* **10**. doi:10.7554/ELIFE.58313
818 Freyberg Z, Sonders MS, Aguilar JI, Hiranita T, Karam CS, Flores J, Pizzo AB, Zhang Y,
819 Farino ZJ, Chen A, Martin CA, Kopajtic TA, Fei H, Hu G, Lin YY, Mosharov E V.,
820 McCabe BD, Freyberg R, Wimalasena K, Hsin LW, Sames D, Krantz DE, Katz JL,
821 Sulzer D, Javitch JA. 2016. Mechanisms of amphetamine action illuminated through
822 optical monitoring of dopamine synaptic vesicles in Drosophila brain. *Nat Commun* **7**.
823 doi:10.1038/ncomms10652
824 Gaudelli NM, Komor AC, Rees HA, Packer MS, Badran AH, Bryson DI, Liu DR. 2017.
825 Programmable base editing of T to G C in genomic DNA without DNA cleavage.
826 *Nature*. doi:10.1038/nature24644
827 Gerfen CR, Surmeier DJ. 2011. Modulation of striatal projection systems by dopamine. *Annu*
828 *Rev Neurosci* **34**:441–466. doi:10.1146/ANNUREV-NEURO-061010-113641
829 Gitler AD, Dhillon P, Shorter J. 2017. Neurodegenerative disease: Models, mechanisms, and
830 a new hope. *DMM Dis Model Mech*. doi:10.1242/dmm.030205
831 Glajch KE, Fleming SM, Surmeier DJ, Osten P. 2012. Sensorimotor assessment of the
832 unilateral 6-hydroxydopamine mouse model of Parkinson's disease. *Behav Brain Res*
833 **230**. doi:10.1016/j.bbr.2011.12.007
834 Gray SJ, Foti SB, Schwartz JW, Bachaboina L, Taylor-Blake B, Coleman J, Ehlers MD,
835 Zylka MJ, McCown TJ, Samulski RJ. 2011. Optimizing promoters for recombinant
836 adeno-associated virus-mediated gene expression in the peripheral and central nervous
837 system using self-complementary vectors. *Hum Gene Ther* **22**.
838 doi:10.1089/hum.2010.245
839 Grieger JC, Samulski RJ. 2005. Packaging Capacity of Adeno-Associated Virus Serotypes:
840 Impact of Larger Genomes on Infectivity and Postentry Steps. *J Virol*.
841 doi:10.1128/jvi.79.15.9933-9944.2005
842 Guo Z, Zhang L, Wu Z, Chen Y, Wang F, Chen G. 2014. In vivo direct reprogramming of
843 reactive glial cells into functional neurons after brain injury and in an Alzheimer's
844 disease model. *Cell Stem Cell* **14**. doi:10.1016/j.stem.2013.12.001
845 Han A, Stoilov P, Linares AJ, Zhou Y, Fu XD, Black DL. 2014. De Novo Prediction of
846 PTBP1 Binding and Splicing Targets Reveals Unexpected Features of Its RNA
847 Recognition and Function. *PLoS Comput Biol* **10**. doi:10.1371/journal.pcbi.1003442
848 Hoang T, Kim DW, Appel H, Ozawa M, Zheng S, Kim J, Blackshaw S. 2023. Ptbp1 deletion
849 does not induce astrocyte-to-neuron conversion. *Nat 2023 6187964* **618**:E1–E7.

bioRxiv preprint doi: https://doi.org/10.1101/2024.03.22.586274; this version posted October 8, 2024. The copyright holder for this preprint (which was not certified by peer review) is the author/funder, who has granted bioRxiv a license to display the preprint in perpetuity. It is made available under aCC-BY 4.0 International license.

doi:10.1038/s41586-023-06066-9

Iancu R, Mohapel P, Brundin P, Paul G. 2005. Behavioral characterization of a unilateral 6-OHDA-lesion model of Parkinson's disease in mice. *Behav Brain Res* **162**. doi:10.1016/j.bbr.2005.02.023

Jiang Y, Wang Y, Huang Z. 2021. Targeting PTB as a One-Step Procedure for In Situ Astrocyte-to-Dopamine Neuron Reprogramming in Parkinson's Disease. *Neurosci Bull* **37**:430. doi:10.1007/S12264-021-00630-X

Kalia L V., Lang AE. 2015. Parkinson's disease. *Lancet*. doi:10.1016/S0140-6736(14)61393-3

Karam CS, Williams BL, Jones SK, Javitch JA. 2022. The Role of the Dopamine Transporter in the Effects of Amphetamine on Sleep and Sleep Architecture in Drosophila. *Neurochem Res* **47**. doi:10.1007/s11064-021-03275-4

Kluesner MG, Lahr WS, Lonetree C lin, Smeester BA, Qiu X, Slipek NJ, Claudio Vázquez PN, Pitzen SP, Pomeroy EJ, Vignes MJ, Lee SC, Bingea SP, Andrew AA, Webber BR, Moriarity BS. 2021. CRISPR-Cas9 cytidine and adenosine base editing of splice-sites mediates highly-efficient disruption of proteins in primary and immortalized cells. *Nat Commun* **12**. doi:10.1038/s41467-021-22009-2

Kluesner MG, Nedveck DA, Lahr WS, Garbe JR, Abrahante JE, Webber BR, Moriarity BS. 2018. EditR: A Method to Quantify Base Editing from Sanger Sequencing. *Cris J* **1**:239–250. doi:10.1089/CRISPR.2018.0014

Koblan LW, Erdos MR, Wilson C, Cabral WA, Levy JM, Xiong Z-M, Tavarez UL, Davison LM, Gete YG, Mao X, Newby GA, Doherty SP, Narisu N, Sheng Q, Krilow C, Lin CY, Gordon LB, Cao K, Collins FS, Brown JD, Liu DR. 2021. In vivo base editing rescues Hutchinson–Gilford progeria syndrome in mice. *Nature*.

Komor AC, Kim YB, Packer MS, Zuris JA, Liu DR. 2016. Programmable editing of a target base in genomic DNA without double-stranded DNA cleavage. *Nature*. doi:10.1038/nature17946

Kosicki M, Tomberg K, Bradley A. 2018. Repair of double-strand breaks induced by CRISPR–Cas9 leads to large deletions and complex rearrangements. *Nat Biotechnol*. doi:10.1038/nbt.4192

Kreitzer AC, Malenka RC. 2008. Striatal Plasticity and Basal Ganglia Circuit Function. *Neuron* **60**:543–554. doi:10.1016/J.NEURON.2008.11.005

Kügler S, Kilic E, Bähr M. 2003. Human synapsin 1 gene promoter confers highly neuron-specific long-term transgene expression from an adenoviral vector in the adult rat brain

bioRxiv preprint doi: https://doi.org/10.1101/2024.03.22.586274; this version posted October 8, 2024. The copyright holder for this preprint (which was not certified by peer review) is the author/funder, who has granted bioRxiv a license to display the preprint in perpetuity. It is made available under aCC-BY 4.0 International license.

884 depending on the transduced area. *Gene Ther*. doi:10.1038/sj.gt.3301905
885 Lee Y, Messing A, Su M, Brenner M. 2008. GFAP promoter elements required for region-
886 specific and astrocyte-specific expression. *Glia* **56**. doi:10.1002/glia.20622
887 Levy JM, Yeh WH, Pendse N, Davis JR, Hennessey E, Butcher R, Koblan LW, Comander J,
888 Liu Q, Liu DR. 2020. Cytosine and adenine base editing of the brain, liver, retina, heart
889 and skeletal muscle of mice via adeno-associated viruses. *Nat Biomed Eng*.
890 doi:10.1038/s41551-019-0501-5
891 Li J, Sun W, Wang B, Xiao X, Liu XQ. 2008. Protein trans-splicing as a means for viral
892 vector-mediated in vivo gene therapy. *Hum Gene Ther*. doi:10.1089/hum.2008.009
893 Li Q, Zheng S, Han A, Lin C-H, Stoilov P, Fu X-D, Black DL. 2014. The splicing regulator
894 PTBP2 controls a program of embryonic splicing required for neuronal maturation. *Elife*
895 **3**. doi:10.7554/elife.01201
896 Lindgren HS, Andersson DR, Lagerkvist S, Nissbrandt H, Cenci MA. 2010. L-DOPA-
897 induced dopamine efflux in the striatum and the substantia nigra in a rat model of
898 Parkinson's disease: Temporal and quantitative relationship to the expression of
899 dyskinesia. *J Neurochem* **112**:1465–1476. doi:10.1111/J.1471-4159.2009.06556.X
900 Makeyev E V., Zhang J, Carrasco MA, Maniatis T. 2007. The MicroRNA miR-124 Promotes
901 Neuronal Differentiation by Triggering Brain-Specific Alternative Pre-mRNA Splicing.
902 *Mol Cell* **27**:435. doi:10.1016/J.MOLCEL.2007.07.015
903 Moore DJ, West AB, Dawson VL, Dawson TM. 2005. MOLECULAR
904 PATHOPHYSIOLOGY OF PARKINSON'S DISEASE. *Annu Rev Neurosci*.
905 doi:10.1146/annurev.neuro.28.061604.135718
906 Musunuru K, Chadwick AC, Mizoguchi T, Garcia SP, DeNizio JE, Reiss CW, Wang K, Iyer
907 S, Dutta C, Clendaniel V, Amaonye M, Beach A, Berth K, Biswas S, Braun MC, Chen
908 HM, Colace T V., Ganey JD, Gangopadhyay SA, Garrity R, Kasiewicz LN, Lavoie J,
909 Madsen JA, Matsumoto Y, Mazzola AM, Nasrullah YS, Nneji J, Ren H, Sanjeev A,
910 Shay M, Stahley MR, Fan SHY, Tam YK, Gaudelli NM, Ciaramella G, Stolz LE,
911 Malyala P, Cheng CJ, Rajeev KG, Rohde E, Bellinger AM, Kathiresan S. 2021. In vivo
912 CRISPR base editing of PCSK9 durably lowers cholesterol in primates. *Nature* **593**.
913 doi:10.1038/s41586-021-03534-y
914 Niu W, Zang T, Smith DK, Vue TY, Zou Y, Bachoo R, Johnson JE, Zhang CL. 2015. SOX2
915 reprograms resident astrocytes into neural progenitors in the adult brain. *Stem Cell*
916 *Reports* **4**. doi:10.1016/j.stemcr.2015.03.006
917 Niu W, Zang T, Zou Y, Fang S, Smith DK, Bachoo R, Zhang CL. 2013. In vivo

bioRxiv preprint doi: https://doi.org/10.1101/2024.03.22.586274; this version posted October 8, 2024. The copyright holder for this preprint (which was not certified by peer review) is the author/funder, who has granted bioRxiv a license to display the preprint in perpetuity. It is made available under aCC-BY 4.0 International license.

reprogramming of astrocytes to neuroblasts in the adult brain. *Nat Cell Biol* **15**. doi:10.1038/ncb2843

Niu Y, Moghimyfiroozabad S, Moghimyfiroozabad A, Tierney TS, Alavian KN. 2021. The factors for the early and late development of midbrain dopaminergic neurons segregate into two distinct evolutionary clusters. *Brain Disord* **1**:100002. doi:10.1016/J.DSCB.2021.100002

Olsson M, Nikkhah G, Bentlage C, Björklund A. 1995. Forelimb akinesia in the rat Parkinson model: Differential effects of dopamine agonists and nigral transplants as assessed by a new stepping test. *J Neurosci* **15**. doi:10.1523/jneurosci.15-05-03863.1995

Paxinos G, Franklin KBJ. 2001. The Mouse Brain in Stereotaxic Coordinates, 2nd edition. *Acad Press*.

Qian C, Dong B, Wang XY, Zhou FQ. 2021. In vivo glial trans-differentiation for neuronal replacement and functional recovery in central nervous system. *FEBS J* **288**:4773–4785. doi:10.1111/FEBS.15681

Qian H, Kang X, Hu J, Zhang D, Liang Z, Meng F, Zhang X, Xue Y, Maimon R, Dowdy SF, Devaraj NK, Zhou Z, Mobley WC, Cleveland DW, Fu XD. 2020. Reversing a model of Parkinson's disease with in situ converted nigral neurons. *Nature*. doi:10.1038/s41586-020-2388-4

Radhiyanti PT, Konno A, Matsuzaki Y, Hirai H. 2021. Comparative study of neuron-specific promoters in mouse brain transduced by intravenously administered AAV-PHP.eB. *Neurosci Lett* **756**:135956. doi:10.1016/J.NEULET.2021.135956

Robel S, Berninger B, Götz M. 2011. The stem cell potential of glia: Lessons from reactive gliosis. *Nat Rev Neurosci*. doi:10.1038/nrn2978

Rothgangl T, Dennis MK, Lin PJC, Oka R, Witzigmann D, Villiger L, Qi W, Hruzova M, Kissling L, Lenggenhager D, Borrelli C, Egli S, Frey N, Bakker N, Walker JA, Kadina AP, Victorov D V., Pacesa M, Kreutzer S, Kontarakis Z, Moor A, Jinek M, Weissman D, Stoffel M, van Boxtel R, Holden K, Pardi N, Thöny B, Häberle J, Tam YK, Semple SC, Schwank G. 2021. In vivo adenine base editing of PCSK9 in macaques reduces LDL cholesterol levels. *Nat Biotechnol*. doi:10.1038/s41587-021-00933-4

Schindelin J, Arganda-Carreras I, Frise E, Kaynig V, Longair M, Pietzsch T, Preibisch S, Rueden C, Saalfeld S, Schmid B, Tinevez JY, White DJ, Hartenstein V, Eliceiri K, Tomancak P, Cardona A. 2012. Fiji: An open-source platform for biological-image analysis. *Nat Methods*. doi:10.1038/nmeth.2019

Shimada IS, LeComte MD, Granger JC, Quinlan NJ, Spees JL. 2012. Self-renewal and

bioRxiv preprint doi: https://doi.org/10.1101/2024.03.22.586274; this version posted October 8, 2024. The copyright holder for this preprint (which was not certified by peer review) is the author/funder, who has granted bioRxiv a license to display the preprint in perpetuity. It is made available under aCC-BY 4.0 International license.

952 differentiation of reactive astrocyte-derived neural stem/progenitor cells isolated from
953 the cortical peri-infarct area after stroke. *J Neurosci* **32**. doi:10.1523/JNEUROSCI.4303-
954 11.2012
955 Shin HY, Wang C, Lee HK, Yoo KH, Zeng X, Kuhns T, Yang CM, Mohr T, Liu C,
956 Hennighausen L. 2017. CRISPR/Cas9 targeting events cause complex deletions and
957 insertions at 17 sites in the mouse genome. *Nat Commun*. doi:10.1038/ncomms15464
958 Sirko S, Behrendt G, Johansson PA, Tripathi P, Costa MR, Bek S, Heinrich C, Tiedt S, Colak
959 D, Dichgans M, Fischer IR, Plesnila N, Staufenbiel M, Haass C, Snapyan M,
960 Saghatelyan A, Tsai LH, Fischer A, Grobe K, Dimou L, Götz M. 2013. Erratum:
961 Reactive glia in the injured brain acquire stem cell properties in response to sonic
962 hedgehog (Cell Stem Cell (2013) 12 426-439)). *Cell Stem Cell*.
963 doi:10.1016/j.stem.2013.04.007
964 Stirling DR, Swain-Bowden MJ, Lucas AM, Carpenter AE, Cimini BA, Goodman A. 2021.
965 CellProfiler 4: improvements in speed, utility and usability. *BMC Bioinformatics* **22**.
966 doi:10.1186/s12859-021-04344-9
967 Stoker TB, Barker RA. 2020. Recent developments in the treatment of Parkinson's Disease.
968 *F1000Research* **9**. doi:10.12688/F1000RESEARCH.25634.1
969 Sun H, Monenschein H, Schiffer HH, Reichard HA, Kikuchi S, Hopkins M, Macklin TK,
970 Hitchcock S, Adams M, Green J, Brown J, Murphy ST, Kaushal N, Collia DR, Moore S,
971 Ray WJ, English NM, Carlton MBL, Brice NL. 2021. First-Time Disclosure of
972 CVN424, a Potent and Selective GPR6 Inverse Agonist for the Treatment of Parkinson's
973 Disease: Discovery, Pharmacological Validation, and Identification of a Clinical
974 Candidate. *J Med Chem* **64**. doi:10.1021/acs.jmedchem.0c02081
975 Torper O, Götz M. 2017. Brain repair from intrinsic cell sources: Turning reactive glia into
976 neuronsProgress in Brain Research. doi:10.1016/bs.pbr.2016.12.010
977 Truong DJJ, Kühner K, Kühn R, Werfel S, Engelhardt S, Wurst W, Ortiz O. 2015.
978 Development of an intein-mediated split-Cas9 system for gene therapy. *Nucleic Acids*
979 *Res*. doi:10.1093/nar/gkv601
980 Tsai SQ, Topkar V V., Joung JK, Aryee MJ. 2016. Open-source guideseq software for
981 analysis of GUIDE-seq data. *Nat Biotechnol 2016 345* **34**:483–483.
982 doi:10.1038/nbt.3534
983 Tsai SQ, Zheng Z, Nguyen NT, Liebers M, Topkar V V., Thapar V, Wyvekens N, Khayter C,
984 Iafrate AJ, Le LP, Aryee MJ, Joung JK. 2014. GUIDE-seq enables genome-wide
985 profiling of off-target cleavage by CRISPR-Cas nucleases. *Nat Biotechnol 2014 332*

bioRxiv preprint doi: https://doi.org/10.1101/2024.03.22.586274; this version posted October 8, 2024. The copyright holder for this preprint (which was not certified by peer review) is the author/funder, who has granted bioRxiv a license to display the preprint in perpetuity. It is made available under aCC-BY 4.0 International license.

**33**:187–197. doi:10.1038/nbt.3117

Valcárcel J, Gebauer F. 1997. Post-transcriptional regulation: The dawn of PTB. *Curr Biol* **7**. doi:10.1016/s0960-9822(06)00361-7

Villiger L, Grisch-Chan HM, Lindsay H, Ringnalda F, Pogliano CB, Allegri G, Fingerhut R, Häberle J, Matos J, Robinson MD, Thöny B, Schwank G. 2018. Treatment of a metabolic liver disease by in vivo genome base editing in adult mice. *Nat Med*. doi:10.1038/s41591-018-0209-1

Wang LL, Serrano C, Zhong X, Ma S, Zou Y, Zhang CL. 2021. Revisiting astrocyte to neuron conversion with lineage tracing in vivo. *Cell* **184**. doi:10.1016/j.cell.2021.09.005

Winter J, Luu A, Gapinske M, Manandhar S, Shirguppe S, Woods WS, Song JS, Perez-Pinera P. 2019. Targeted exon skipping with AAV-mediated split adenine base editors. *Cell Discov* **5**. doi:10.1038/s41421-019-0109-7

Xue Y, Ouyang K, Huang J, Zhou Y, Ouyang H, Li H, Wang G, Wu Q, Wei C, Bi Y, Jiang L, Cai Z, Sun H, Zhang K, Zhang Y, Chen J, Fu XD. 2013. Direct conversion of fibroblasts to neurons by reprogramming PTB-regulated MicroRNA circuits. *Cell*. doi:10.1016/j.cell.2012.11.045

Xue Y, Qian H, Hu J, Zhou B, Zhou Y, Hu X, Karakhanyan A, Pang Z, Fu XD. 2016. Sequential regulatory loops as key gatekeepers for neuronal reprogramming in human cells. *Nat Neurosci 2016 196* **19**:807–815. doi:10.1038/nn.4297

Yang G, Yan Z, Wu X, Zhang M, Xu C, Shi L, Yang H, Fang K. 2023. Ptbp1 knockdown failed to induce astrocytes to neurons in vivo. *Gene Ther 2023* 1–6. doi:10.1038/s41434-023-00382-5

Yu GL, Zhang Y, Ning B. 2021. Reactive Astrocytes in Central Nervous System Injury: Subgroup and Potential Therapy. *Front Cell Neurosci*. doi:10.3389/fncel.2021.792764

Yu X, Nagai J, Khakh BS. 2020. Improved tools to study astrocytes. *Nat Rev Neurosci*. doi:10.1038/s41583-020-0264-8

Zheng S, Gray EE, Chawla G, Porse BT, O'Dell TJ, Black DL. 2012. Psd-95 is post-transcriptionally repressed during early neural development by PTBP1 and PTBP2. *Nat Neurosci* **15**:381. doi:10.1038/NN.3026

Zhou H, Su J, Hu X, Zhou C, Li H, Chen Z, Xiao Q, Wang B, Wu W, Sun Y, Zhou Y, Tang C, Liu F, Wang L, Feng C, Liu M, Li S, Zhang Y, Xu H, Yao H, Shi L, Yang H. 2020. Glia-to-Neuron Conversion by CRISPR-CasRx Alleviates Symptoms of Neurological Disease in Mice. *Cell*. doi:10.1016/j.cell.2020.03.024

bioRxiv preprint doi: https://doi.org/10.1101/2024.03.22.586274; this version posted October 8, 2024. The copyright holder for this preprint (which was not certified by peer review) is the author/funder, who has granted bioRxiv a license to display the preprint in perpetuity. It is made available under aCC-BY 4.0 International license.

## Figures and figure supplements

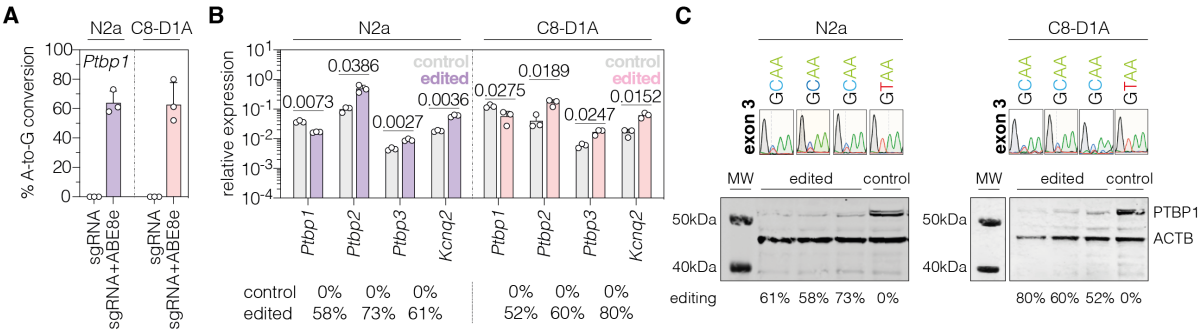


**Figure 1 | PTBP1 downregulation by adenine base editing with sgRNA-ex3 in neuronal and astroglial cell lines. (A)** Editing rates at the *Ptbp1* splice donor of exon 3 in N2a and C8-D1A cell lines. Editing efficiencies were determined by Sanger sequencing and EditR (Kluesner et al., 2018). Control samples were transfected with sgRNA (gray). **(B)** Transcript levels of *Ptbp1* and *Ptbp1*-repressed exons upon adenine base editing in N2a and C8-D1A cells. Transcripts were normalized to *Gapdh*. **(C)** PTBP1 levels in control (1 independent experiment) and edited N2a or C8-D1A cells (3 independent experiments). ACTB protein levels are shown as a loading control. Corresponding sequencing chromatograms for sgRNA-ex3 are shown above each sample. Corresponding editing rates are shown below the plots in (B) and (C). Normal distribution of the data was analyzed using the Shapiro-Wilk test. Data are represented as means±s.d. of three independent experiments (A,B) and were analyzed using an unpaired two-tailed Student's t-test with Welch's correction (B). Each datapoint represents one independent experiment. Exact *P*-values are indicated in the respective plots. *Ptbp1*, Polypyrimidine tract binding protein 1; *Ptbp2*, Polypyrimidine tract binding protein 2; *Ptbp3*, Polypyrimidine tract binding protein 3; *Kcnq2*, potassium voltage-gates channel subfamily Q member 2; MW, molecular weight marker; kDa, kilodalton.

bioRxiv preprint doi: https://doi.org/10.1101/2024.03.22.586274; this version posted October 8, 2024. The copyright holder for this preprint (which was not certified by peer review) is the author/funder, who has granted bioRxiv a license to display the preprint in perpetuity. It is made available under aCC-BY 4.0 International license.

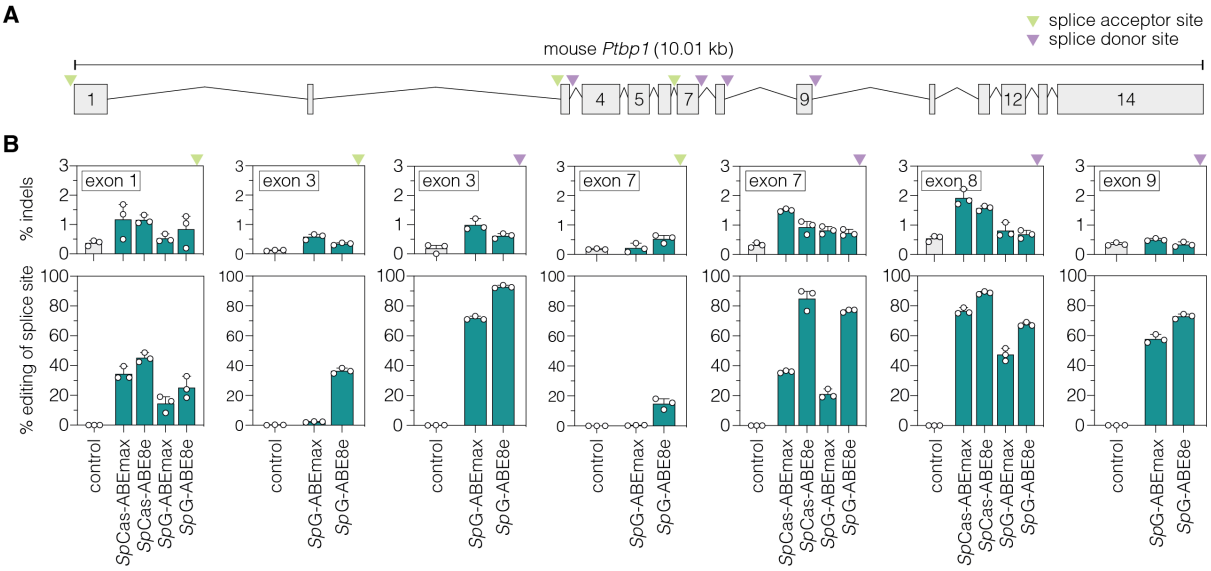


**Figure 1 – figure supplement 1 | Adenine base editing of *Ptbp1* splice sites in murine Hepa cells. (A)** Schematic overview of exons and introns of the targeted murine *Ptbp1* locus. sgRNAs target either the conserved GT motif of canonical splice donor sites at the beginning of an intron (purple arrowhead) or the conserved AG motif of canonical splice acceptor sites at the end of an intron (green arrowhead). **(B)** Editing of adenines and indel rates at *Ptbp1* splice donor (purple arrowhead) or acceptor sites (green arrowhead) for *Sp*Cas- or *Sp*G-ABE variants (teal). The targeted exons are indicated in the respective plot. Control samples were transfected with sgRNA (gray). Data are displayed as means±s.d. of three independent experiments. Each datapoint represents one independent experiment. *Ptbp1*, polypyrimidine tract binding protein 1; kb, kilobases; *Sp*Cas, *Streptococcus pyogenes* Cas9 recognizing NGG PAMs; *Sp*G, *Sp*Cas variant recognizing NGN PAMs.

bioRxiv preprint doi: https://doi.org/10.1101/2024.03.22.586274; this version posted October 8, 2024. The copyright holder for this preprint (which was not certified by peer review) is the author/funder, who has granted bioRxiv a license to display the preprint in perpetuity. It is made available under aCC-BY 4.0 International license.

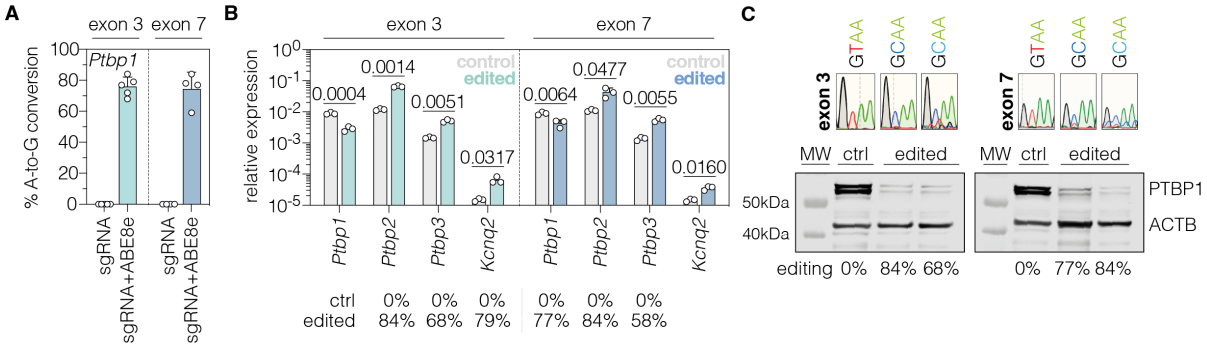


**Figure 1 – figure supplement 2 | *In vitro* validation of PTBP1 repression by adenine base editing with sgRNA-ex3 or sgRNA-ex7 in Hepa cells. (A)** Editing rates at *Ptbp1* splice donor sites of exon 3 and exon 7. Editing efficiencies were determined by Sanger sequencing and EditR (Kluesner et al., 2018). Control samples were transfected with sgRNA (gray). **(B)** Transcript levels of *Ptbp1* and *Ptbp1*-repressed exons upon adenine base editing in Hepa cells. Transcripts were normalized to *Gapdh*. **(C)** PTBP1 levels in control (1 independent experiment) and edited Hepa cells (2 independent experiments). ACTB protein levels are shown as a loading control. Corresponding sequencing chromatograms for sgRNA-ex3 and sgRNA-ex7 are shown above each sample. Corresponding editing rates are shown below the plots in (B) and (C). Normal distribution of the data was analyzed using the Shapiro-Wilk test. Data are represented as means±s.d. of at least three independent experiments (A,B) and were analyzed using an unpaired two-tailed Student's t-test with Welch's correction (B). Each datapoint represents one independent experiment. Exact *P*-values are indicated in the respective plots. *Ptbp1*, Polypyrimidine tract binding protein 1; *Ptbp2*, Polypyrimidine tract binding protein 2; *Ptbp3*, Polypyrimidine tract binding protein 3; *Kcnq2*, potassium voltage-gates channel subfamily Q member 2; ctrl, control; MW, molecular weight marker.

bioRxiv preprint doi: https://doi.org/10.1101/2024.03.22.586274; this version posted October 8, 2024. The copyright holder for this preprint (which was not certified by peer review) is the author/funder, who has granted bioRxiv a license to display the preprint in perpetuity. It is made available under aCC-BY 4.0 International license.

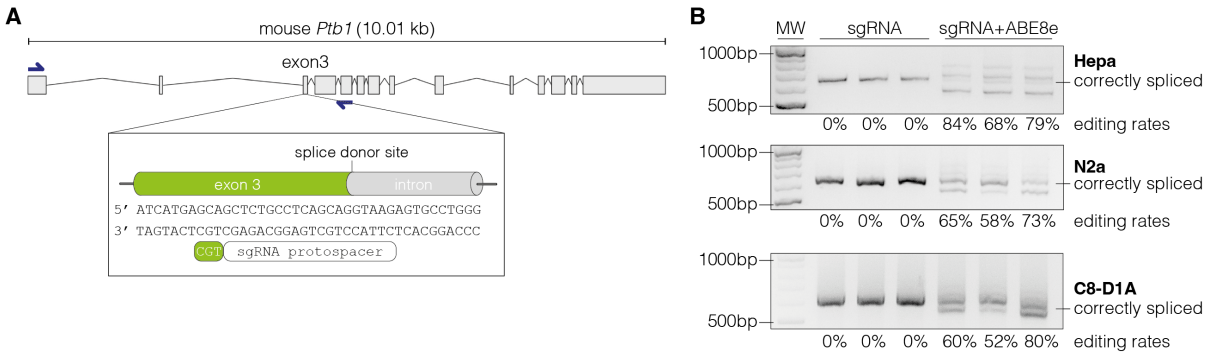


**Figure 1 – figure supplement 3 | Adenine base editing generates alternative *Ptbp1* splice sites in cell lines. (A)** Schematic representation of the splice donor at the exon-intron junction of *Ptbp1* exon 3. **(B)** Editing of the canonical splice donor at exon 3 generates alternative *Ptbp1* splice sites in Hepa, N2a, and C8-D1A cells. The correctly spliced isoform is labelled. The corresponding editing rates are shown below each plot. Data of three independent experiments are shown (B). Size of molecular weight (MW) markers in basepairs (bp) are indicated in (B).

bioRxiv preprint doi: https://doi.org/10.1101/2024.03.22.586274; this version posted October 8, 2024. The copyright holder for this preprint (which was not certified by peer review) is the author/funder, who has granted bioRxiv a license to display the preprint in perpetuity. It is made available under aCC-BY 4.0 International license.

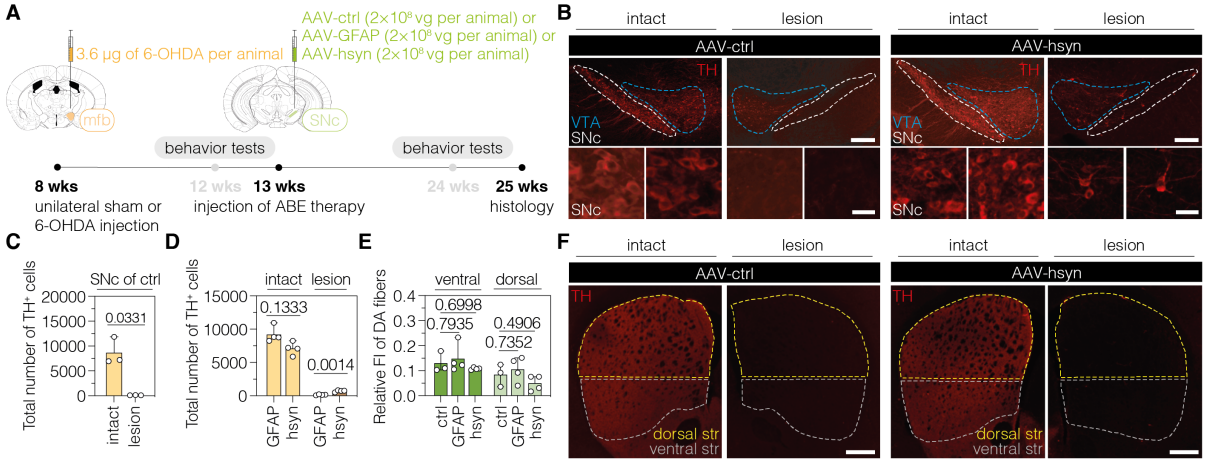


**Figure 2 | Downregulation of PTBP1 in neurons of the SNc generates TH$^+$ cells. (A)** Schematic representation of the experimental timeline and setup. **(B)** Representative images of midbrain sections showing the intact (left) or lesioned (right) SNc in animals treated with AAV-ctrl (left) or AAV-hsyn (right). Treatment groups and hemispheres are indicated on top. **(C,D)** Quantification of TH$^+$ cells in the intact or lesioned SNc in animals treated with AAV-ctrl (C), AAV-GFAP (D), or AAV-hsyn (D) in the lesioned hemisphere. **(E,F)** Quantifications (E) of DA fibers in the striatum, assessed as relative fluorescence intensity (FI) of TH compared to the intact striatum of the same section, and representative images of brain sections (F) showing the intact or denervated striatum (str) in animals treated with AAV-ctrl (left) or AAV-hsyn (right). The FI of the TH staining detected in the corpus callosum of each hemisphere was used for background correction of FI detected in the striatum of the same hemisphere. Control animals were treated with AAV-PHP.eB particles, expressing the ABE8e variant under the ubiquitous Cbh promoter. Tissue areas used for quantifications are marked by colored dashed lines in (B) and (E). Normal distribution of the data was analyzed using the Shapiro-Wilk test. Data are represented as means±s.d. of 3-8 animals per group and were analyzed using an unpaired two-tailed Student's t-test with Welch's correction (C, D) or a one-way ANOVA with Dunnett's multiple comparisons test (E). Each datapoint represents one animal. Exact *P*-values are indicated in the respective plots. Scale bars, 20 µm (B, bottom) and 1000 µm (B, top; F). ctrl, AAV-ctrl-ABE treatment; GFAP, AAV-GFAP-ABE treatment; hsyn, AAV-hsyn-ABE treatment; ABE, adenine base editor; vg, vector genomes; SNc, substantia nigra pars compacta; VTA, ventral tegmental area; TH, tyrosine hydroxylase; str, striatum; FI, fluorescence intensity; DA, dopaminergic.

bioRxiv preprint doi: https://doi.org/10.1101/2024.03.22.586274; this version posted October 8, 2024. The copyright holder for this preprint (which was not certified by peer review) is the author/funder, who has granted bioRxiv a license to display the preprint in perpetuity. It is made available under aCC-BY 4.0 International license.

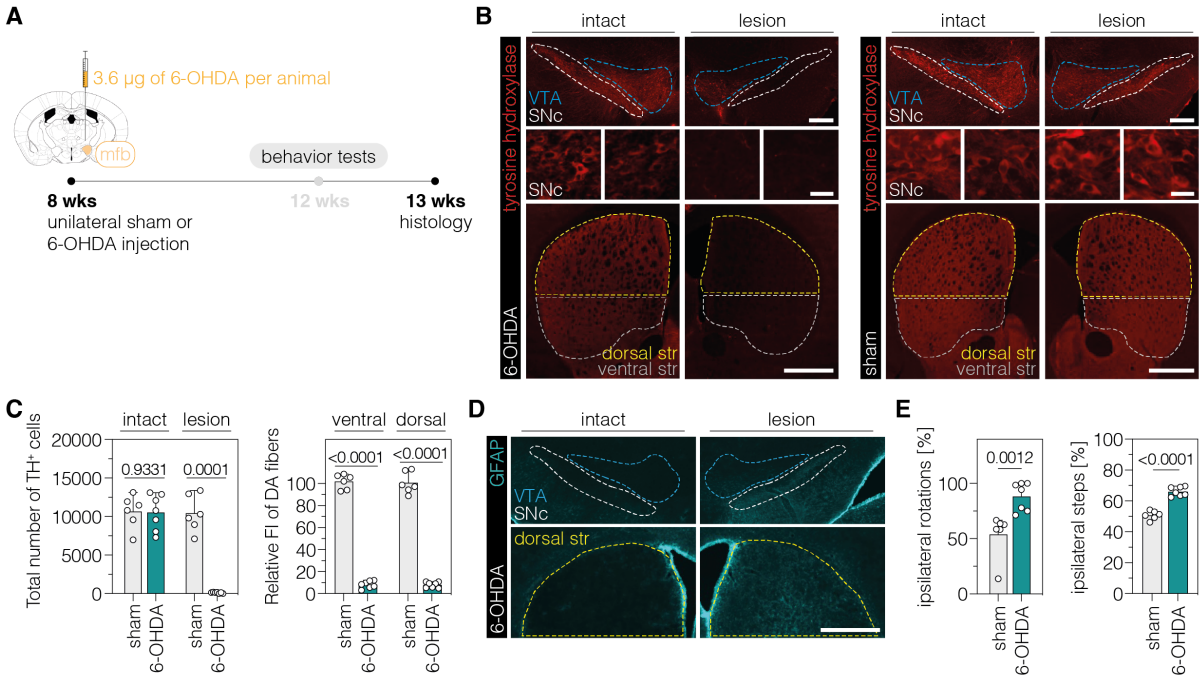


**Figure 2 – figure supplement 1 | Validation of the unilateral 6-OHDA lesion in C57BL/6J mice. (A)** Schematic representation of the experimental timeline and setup. **(B)** Representative fluorescence images showing the unilateral loss of $TH^+$ cells in the SNc (top and middle) and unilateral depletion of DA fibers in the striatum (bottom) in 6-OHDA-lesioned mice (left). Sham-injected animals (right) are shown for comparison. The FI of the TH staining detected in the corpus callosum of each hemisphere was used for background correction of FI detected in the striatum of the same hemisphere. Treatment groups are indicated on the left. **(C)** Quantifications of $TH^+$ DANs in the SNc (left) and DA fibers in the ventral and dorsal striatum (right). Tissue areas used for quantifications are marked by colored dashed lines in (B). **(D)** Unilateral activation of astrocytes in the SNc (top) and dorsal striatum (bottom) in 6-OHDA-lesioned mice. **(E)** Spontaneous behaviors in sham- and 6-OHDA-lesioned mice. Normal distribution of the data was analyzed using the Shapiro-Wilk test. Data are displayed as means±s.d. of 6-7 mice per group and were analyzed using an unpaired two-tailed Student's t-test with Welch's correction (C, ipsilateral steps in E) or a two-tailed Mann Whitney test (ipsilateral rotations in E). Each datapoint represents one animal. Exact *P*-values are indicated in the respective plots. Scale bars, 20 µm (B, bottom) and 1000 µm (B, top; D). FI, fluorescence intensity; SNc, substantia nigra pars compacta; str, striatum; VTA, ventral tegmental area; GFAP, glial fibrillary acidic protein; TH, tyrosine hydroxylase; DA, dopaminergic.

bioRxiv preprint doi: https://doi.org/10.1101/2024.03.22.586274; this version posted October 8, 2024. The copyright holder for this preprint (which was not certified by peer review) is the author/funder, who has granted bioRxiv a license to display the preprint in perpetuity. It is made available under aCC-BY 4.0 International license.

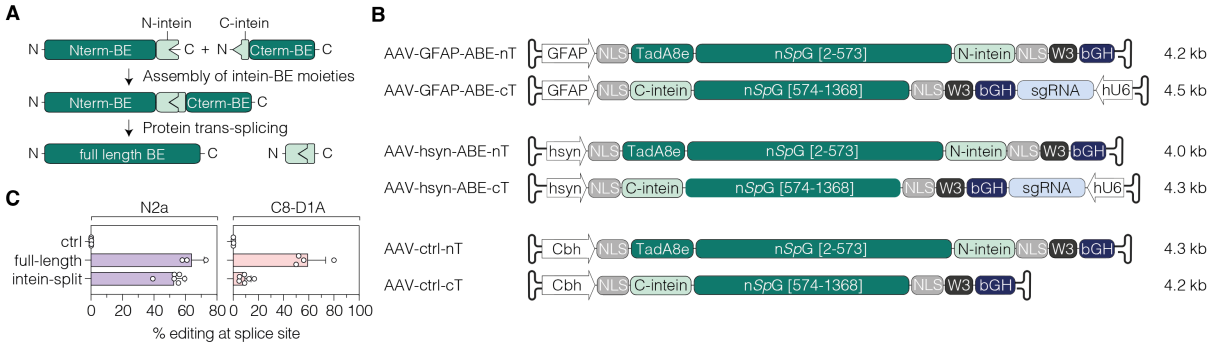


**Figure 2 – figure supplement 2 | AAV vector designs for neuronal or astroglial expression of intein-split ABE8e. (A)** Depiction of *Npu* intein-split BE moieties (Nterm-BE and Cterm-BE), forming the full length BE after protein trans-splicing. **(B)** Schematic representation of AAV vector designs with the short GFAP (Lee et al., 2008), hsyn (Kügler et al., 2003), or Cbh promoter (Gray et al., 2011) and their corresponding lengths in kilobase pairs (including ITRs). Constructs are not depicted to scale. **(C)** Editing efficiencies of full-length (CMV promoter) or intein-split ABE expression vectors in N2a (hsyn promoter) and C8-D1A cells (GFAP promoter). Control samples were treated with the sgRNA only. Data of 3-6 independent experiments are displayed as means±s.d. (C). BE, base editor; ABE, adenine base editor; nT/Nterm, N-terminal AAV construct; cT/Cterm, C-terminal AAV construct; GFAP, glial fibrillary acidic protein promoter; hsyn, human synapsin 1 promoter; Cbh, truncated chimeric CMV/chicken b-actin hybrid promoter; NLS, nuclear localization signal; TadA8e, adenosine deaminase; n*Sp*G, *Sp*G nickase; W3, woodchuck hepatitis virus post-transcriptional regulatory element; bGH, bovine growth hormone poly adenylation signal; hU6, human U6 promoter; kb, kilobase pairs.

bioRxiv preprint doi: https://doi.org/10.1101/2024.03.22.586274; this version posted October 8, 2024. The copyright holder for this preprint (which was not certified by peer review) is the author/funder, who has granted bioRxiv a license to display the preprint in perpetuity. It is made available under aCC-BY 4.0 International license.

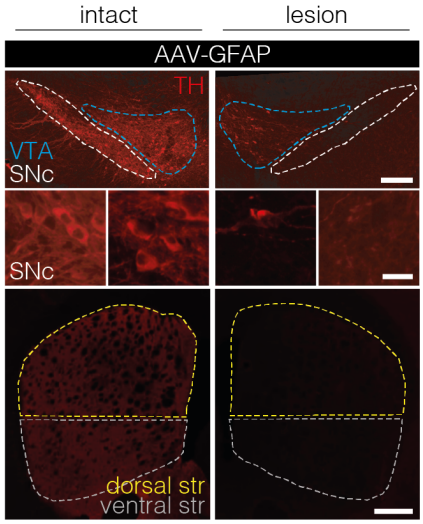


**Figure 2 - figure supplement 3 | PTBP1 downregulation in astrocytes of the SNc fails to generate TH$^+$ cells.** Representative images of brain sections showing the intact (left) or lesioned (right) SNc (top and middle) or striatum (bottom) in animals after astroglial PTBP1 downregulation (n=4 mice). The FI of the TH staining detected in the corpus callosum of each hemisphere was used for background correction of FI detected in the striatum of the same hemisphere. Tissue areas used for quantifications are marked by colored dashed lines. Scale bars, 20 µm (middle) and 1000 µm (top and bottom). AAV-GFAP, AAV-GFAP-ABE treatment; GFAP, glial fibrillary acidic protein; SNc, substantia nigra pars compacta; VTA, ventral tegmental area; TH, tyrosine hydroxylase.

bioRxiv preprint doi: https://doi.org/10.1101/2024.03.22.586274; this version posted October 8, 2024. The copyright holder for this preprint (which was not certified by peer review) is the author/funder, who has granted bioRxiv a license to display the preprint in perpetuity. It is made available under aCC-BY 4.0 International license.

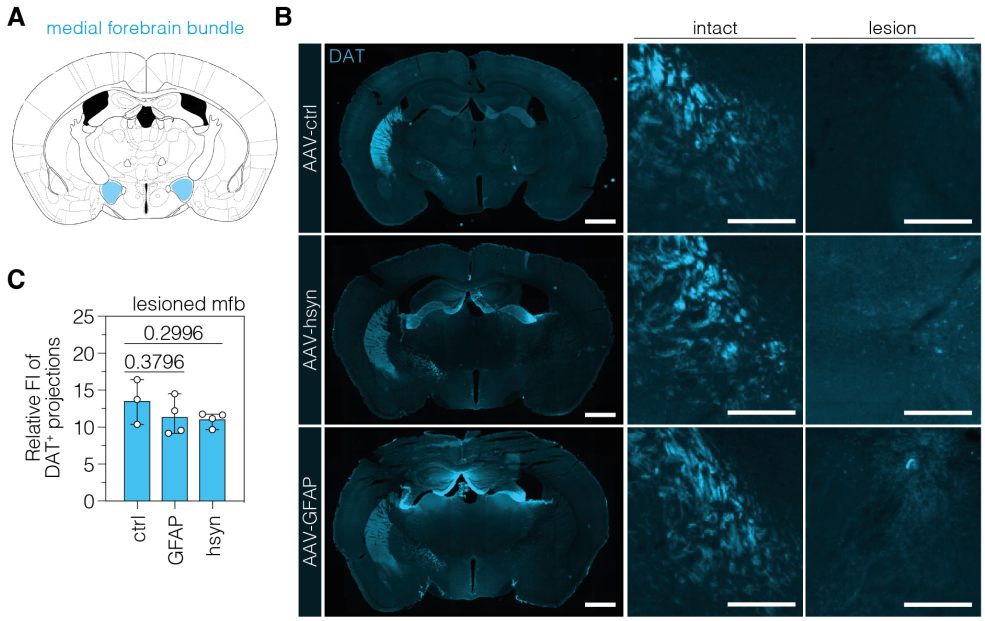


**Figure 2 - figure supplement 4 | TH-expressing cells in the SNc do not form neuronal projections through the mfb. (A,B)** Schematic depiction of the mfb (A) on the mouse brain atlas (Paxinos and Franklin, 2001) and representative images of DA projections in the mfb of the intact and lesioned hemisphere in treated PD mice. Treatment groups (left) and hemispheres (top) are indicated. **(C)** Quantifications of DA projections in the mfb, assessed as relative fluorescence intensity (FI) of the dopaminergic marker DAT (dopamine transporter) compared to the intact mfb of the same section, in animals treated with AAV-ctrl, AAV-GFAP, or AAV-hsyn. The FI of the DAT staining detected in the thalamus of each hemisphere was used for background correction of FI detected in the mfb of the same hemisphere. Control animals were treated with AAV-PHP.eB particles, expressing the ABE8e variant under the ubiquitous Cbh promoter. Normal distribution of the data was analyzed using the Shapiro-Wilk test. Data are represented as means±s.d. of 3-4 animals per group and were analyzed using a one-way ANOVA with Dunnett's multiple comparisons test. Each datapoint represents one animal. Exact *P*-values are indicated in the respective plots. Scale bars, 1000 µm (left) and 50 µm (middle and right). ctrl, AAV-ctrl-ABE treatment; GFAP, AAV-GFAP-ABE treatment; hsyn, AAV-hsyn-ABE treatment; mfb, medial forebrain bundle; FI, fluorescence intensity; DA, dopaminergic; DAT, dopamine transporter.

bioRxiv preprint doi: https://doi.org/10.1101/2024.03.22.586274; this version posted October 8, 2024. The copyright holder for this preprint (which was not certified by peer review) is the author/funder, who has granted bioRxiv a license to display the preprint in perpetuity. It is made available under aCC-BY 4.0 International license.

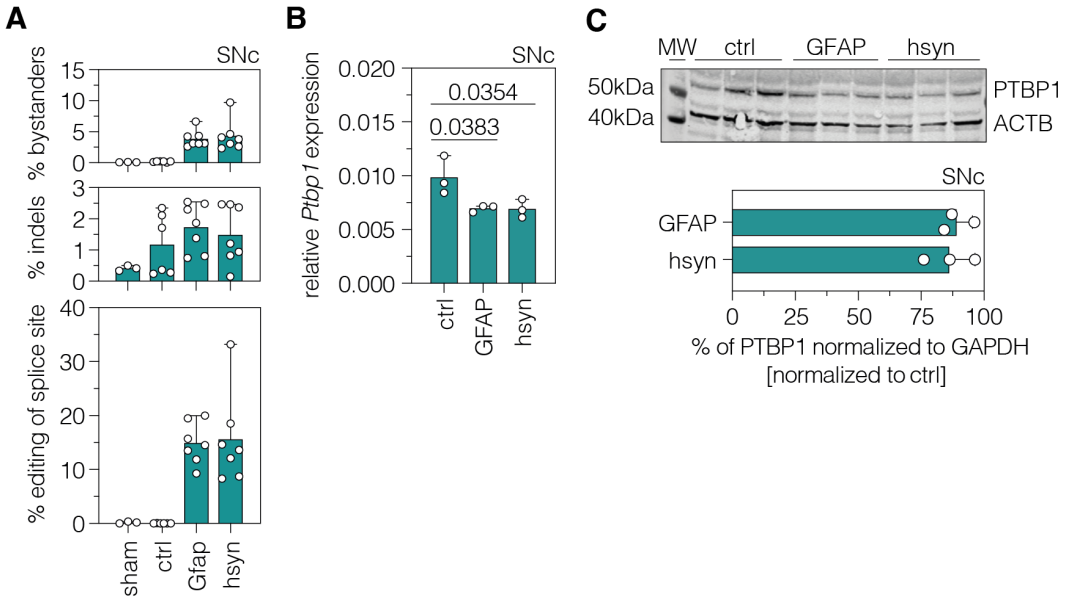


**Figure 2 – figure supplement 5 | *In vivo* validation of PTBP1 downregulation by adenine base editing in astrocytes and neurons of the SNc. (A)** Quantifications of *in vivo* base editing of adenines and indel rates within the editing window at the targeted *Ptbp1* splice donor. **(B)** Transcript levels of *Ptbp1* upon adenine base editing in the lesioned SNc of AAV-ctrl-, AAV-GFAP-, and AAV-hsyn-treated PD mice. Transcripts were normalized to *Gapdh*. **(C)** PTBP1 levels in the lesioned SNc of treated 6-OHDA-lesioned PD mice (n=3 mice per group). ACTB protein levels are shown as a loading control. PTBP1 abundance was compared to ACTB and normalized to the PTBP1/ACTB ratio of AAV-ctrl-treated animals. Control animals were treated with AAV-PHP.eB particles, expressing the ABE8e variant under the ubiquitous Cbh promoter. Normal distribution of the data was analyzed using the Shapiro-Wilk test. Data are represented as means±s.d. of 3-7 animals per group and were analyzed using a one-way ANOVA with Dunnett's multiple comparisons test (C). Each datapoint represents one animal. Exact *P*-values are indicated in the respective plots. ctrl, AAV-ctrl-ABE treatment; GFAP, AAV-GFAP-ABE treatment; hsyn, AAV-hsyn-ABE treatment; SNc, substantia nigra pars compacta; *Ptbp1*/PTBP1, Polypyrimidine tract binding protein 1; ACTB, beta actin; MW, molecular weight marker.

bioRxiv preprint doi: https://doi.org/10.1101/2024.03.22.586274; this version posted October 8, 2024. The copyright holder for this preprint (which was not certified by peer review) is the author/funder, who has granted bioRxiv a license to display the preprint in perpetuity. It is made available under aCC-BY 4.0 International license.

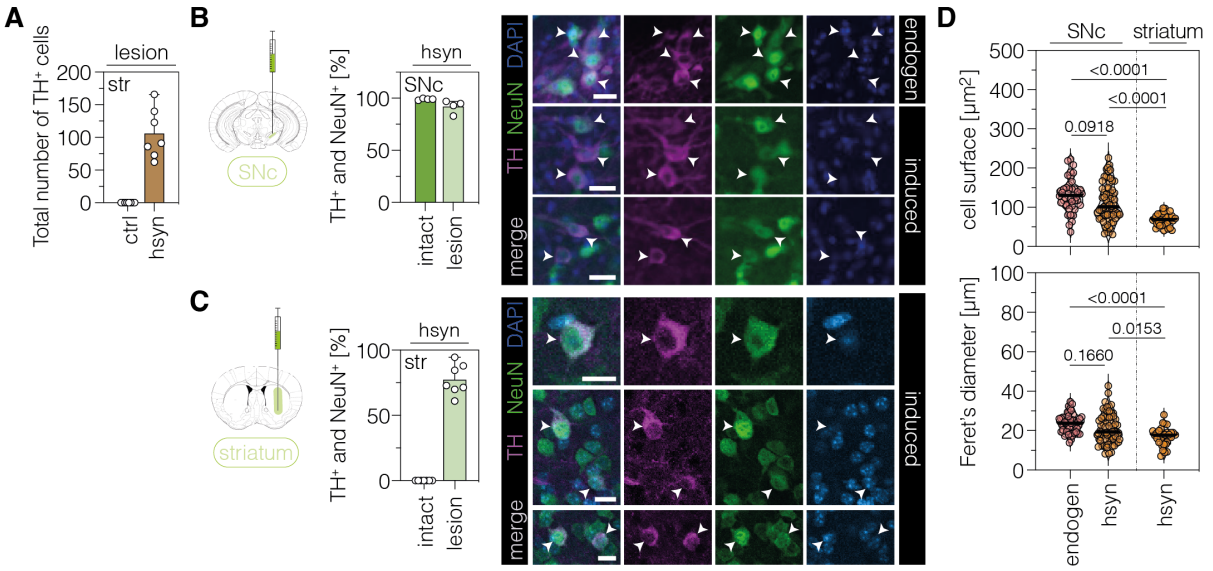


**Figure 3 | Characterization of TH-expressing cells in the SNc or striatum. (A)** Quantification of $TH^+$ cells in the lesioned striatum of animals treated with AAV-ctrl or AAV-hsyn. Control animals were treated with AAV-PHP.eB particles, expressing the ABE8e-*Sp*G variant under the ubiquitous Cbh promoter. **(B,C)** Quantifications (left) and representative images (right) of TH/NeuN double-positive cell bodies in the intact (dark green, labelled as "endogen" in the images) or lesioned (light green, labelled as "induced" in the images) SNc (B) or striatum (C) of AAV-hsyn-treated animals. **(D)** Corresponding quantifications of cell surface area and Feret's diameter (longest distance between the cell boundaries) of TH/NeuN double-positive cell bodies in the intact (labeled as "endogen") or lesioned SNc or striatum (labeled as "hsyn"). Normal distribution of the data was analyzed using the Shapiro-Wilk test. Data are displayed as means±s.d. of 4-7 mice per group (A-C) or 32-68 TH/NeuN double-positive cells per group (D; n=4 mice) and were analyzed using a one-way ANOVA with Tukey's multiple comparisons test (D). Each datapoint represents one animal (A-C) or a TH/NeuN double-positive cell (D). Exact *P*-values are indicated in the each plot above the respective group (D). Scale bars, 20 µm. ctrl, AAV-ctrl-ABE treatment; hsyn, AAV-hsyn-ABE treatment; SNc, substantia nigra pars compacta; str, striatum; TH, tyrosine hydroxylase; NEUN, hexaribonucleotide binding protein-3; DAPI, 4',6-diamidino-2-phenylindole; endogen, endogenous.

bioRxiv preprint doi: https://doi.org/10.1101/2024.03.22.586274; this version posted October 8, 2024. The copyright holder for this preprint (which was not certified by peer review) is the author/funder, who has granted bioRxiv a license to display the preprint in perpetuity. It is made available under aCC-BY 4.0 International license.

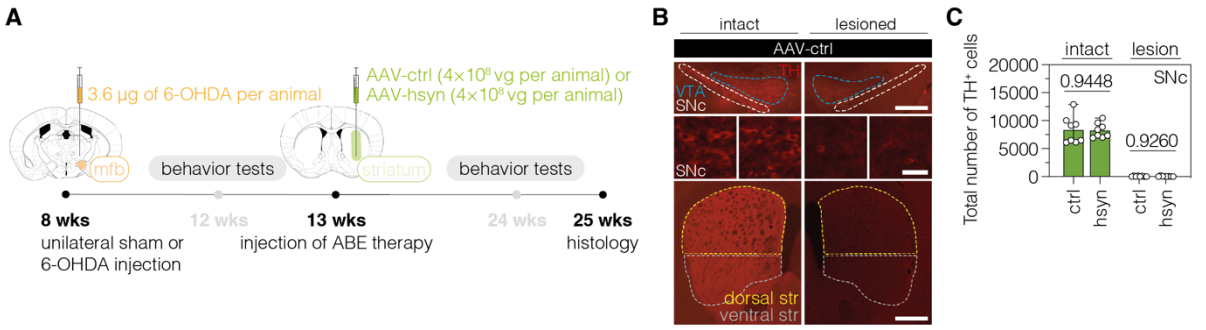


**Figure 3 – figure supplement 1 | Validation of the unilateral lesion in 6-OHDA mice after neuronal PTBP1 downregulation in the striatum. (A)** Schematic representation of the experimental timeline and setup. **(B)** Representative fluorescence images showing the unilateral loss of $TH^+$ cells in the SNc (top and middle) and unilateral depletion of DA fibers in the striatum (bottom) in 6-OHDA-lesioned mice treated with AAV-ctrl. Scale bars, 1000 µm (top and bottom) and 20 µm (middle). **(C)** Quantifications of $TH^+$ cells in the intact (dark green) and lesioned (light green) SNc after administration of the AAV-hsyn treatment to the striatum. Control animals were treated with AAV-PHP.eB particles, expressing the ABE8e-*Sp*G variant under the Cbh promoter. Tissue areas used for quantifications are marked by colored dashed lines in (B). Normal distribution of the data was analyzed using the Shapiro-Wilk test. Data are displayed as means±s.d. of 8 mice per group and were analyzed using an unpaired two-tailed Student's t-test with Welch's correction (C, "intact") or a two-tailed Mann-Whitney test (C, "lesion"). Each datapoint represents one animal. Exact *P*-values are indicated in the respective plots. ABE, adenine base editor; ctrl, AAV-ctrl-ABE treatment; hsyn, AAV-hsyn-ABE treatment; SNc, substantia nigra pars compacta; VTA, ventral tegmental area; TH, tyrosine hydroxylase.

bioRxiv preprint doi: https://doi.org/10.1101/2024.03.22.586274; this version posted October 8, 2024. The copyright holder for this preprint (which was not certified by peer review) is the author/funder, who has granted bioRxiv a license to display the preprint in perpetuity. It is made available under aCC-BY 4.0 International license.


**Figure 3 – figure supplement 2 | *In vivo* validation of PTBP1 downregulation by adenine base editing in neurons of the striatum. (A)** Quantifications of *in vivo* base editing of adenines and indel rates within the editing window at the targeted *Ptbp1* splice donor (n=6-11 mice per group). **(B)** Representative CRISPResso output file showing the frequency and positioning of edited adenines in the lesioned striatum. **(C)** Transcript levels of *Ptbp1* upon adenine base editing in the lesioned striatum. Transcripts were normalized to *Gapdh* (n=3 mice per group). **(D)** PTBP1 levels in the lesioned striatum of treated 6-OHDA-lesioned PD mice (n=3 mice per group). ACTB protein levels are shown as a loading control. PTBP1 abundance was compared to ACTB and normalized to the PTBP1/ACTB ratio of AAV-ctrl-treated animals. Control animals were treated with AAV-PHP.eB particles, expressing the ABE8e variant under the ubiquitous Cbh promoter. Normal distribution of the data was analyzed using the Shapiro-Wilk test. Data are represented as means±s.d. of 3-11 animals per group and were analyzed using an unpaired two-tailed Student's t-test with Welch's correction (B). Each datapoint represents one animal. Exact *P*-values are indicated in the respective plots. ctrl, AAV-ctrl-ABE treatment; hsyn, AAV-hsyn-ABE treatment; str, striatum; *Ptbp1*/PTBP1, Polypyrimidine tract binding protein 1; ACTB, beta actin; MW, molecular weight marker.

bioRxiv preprint doi: https://doi.org/10.1101/2024.03.22.586274; this version posted October 8, 2024. The copyright holder for this preprint (which was not certified by peer review) is the author/funder, who has granted bioRxiv a license to display the preprint in perpetuity. It is made available under aCC-BY 4.0 International license.

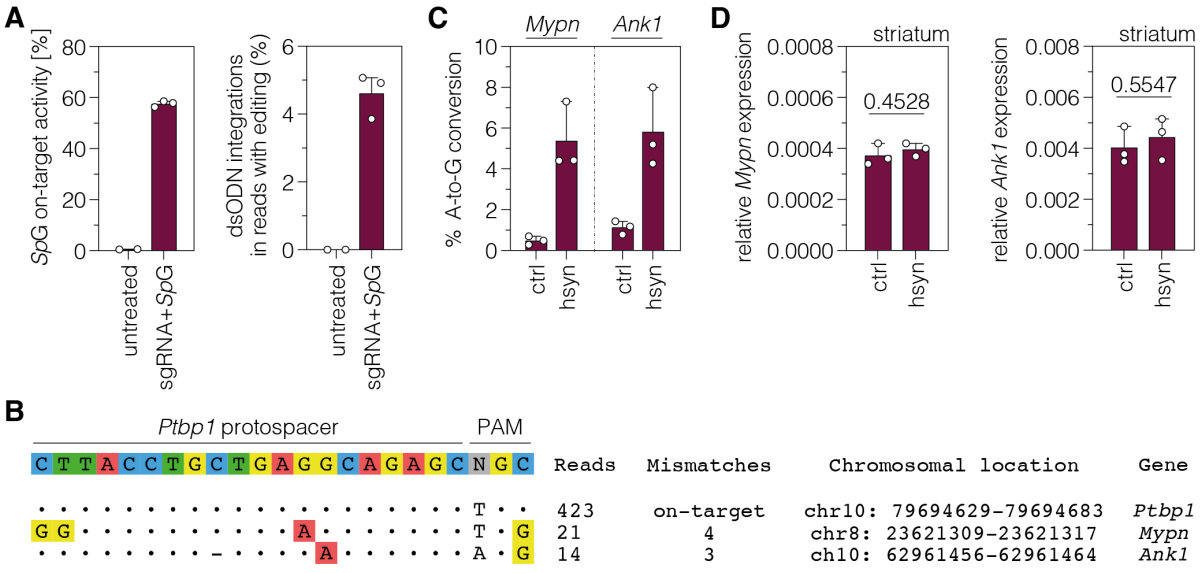


**Figure 3 – figure supplement 3 | Identification of sgRNA-dependent off-target sites using GUIDE-seq. (A)** Frequency of indels of sgRNA-ex3 and the *Sp*G nuclease (left) and dsODN integrations within the edited reads (right) in N2a cells. **(B)** Experimentally identified off-target sites for the sgRNA-ex3 protospacer targeting the *Ptbp1* locus. The number of reads for the on-target (top) and off-target sites (middle and bottom) as well as the number of mismatches, chromosomal location, and gene annotation are indicated on the right. **(C,D)** Deep sequencing results of the off-target sites (C) and transcript levels (D) of *Mypn* and *Ank1* upon adenine base editing in the lesioned striatum. Transcripts were normalized to *Gapdh* (n=3 mice per group). Data are represented as means±s.d. of 3 animals per group and were analyzed using an unpaired two-tailed Student's t-test with Welch's correction (D).

bioRxiv preprint doi: https://doi.org/10.1101/2024.03.22.586274; this version posted October 8, 2024. The copyright holder for this preprint (which was not certified by peer review) is the author/funder, who has granted bioRxiv a license to display the preprint in perpetuity. It is made available under aCC-BY 4.0 International license.

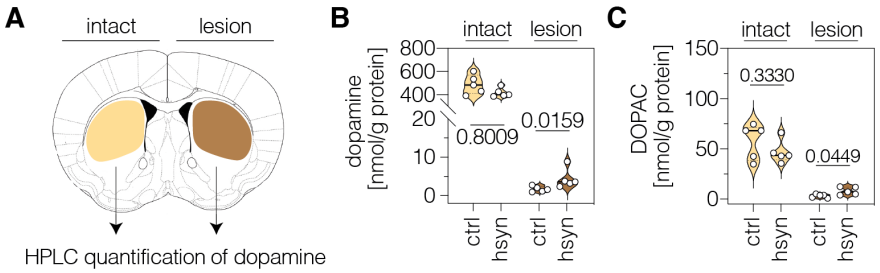


**Figure 3 – figure supplement 4 | Neuronal PTBP1 repression in the striatum increases striatal dopamine in 6-OHDA-lesioned hemispheres. (A)** Schematic representation of striatal regions used for neurotransmitter quantifications. (**B,C**) HPLC quantifications of dopamine (B) and its metabolite DOPAC (C) in the intact and lesioned striatum of animals treated with AAV-ctrl or AAV-hsyn. Control animals were treated with AAV-PHP.eB particles, expressing the ABE8e-*Sp*G variant under the Cbh promoter. Neurotransmitter concentrations in nmol were normalized to total protein amounts in g. Normal distribution of the data was analyzed using the Shapiro-Wilk test. Data are displayed as means±s.d. of 5 mice per group and were analyzed using an unpaired two-tailed Student's t-test ("intact" in B; C) or a two-tailed Mann-Whitney test ("lesion" in B). Each datapoint represents one animal. Exact *P*-values are indicated in the respective plots. ctrl, AAV-ctrl-ABE treatment; hsyn, AAV-hsyn-ABE treatment; DOPAC, 3,4-dihydroxyphenylacetic acid; nmol, nanomol; g, gram.

bioRxiv preprint doi: https://doi.org/10.1101/2024.03.22.586274; this version posted October 8, 2024. The copyright holder for this preprint (which was not certified by peer review) is the author/funder, who has granted bioRxiv a license to display the preprint in perpetuity. It is made available under aCC-BY 4.0 International license.

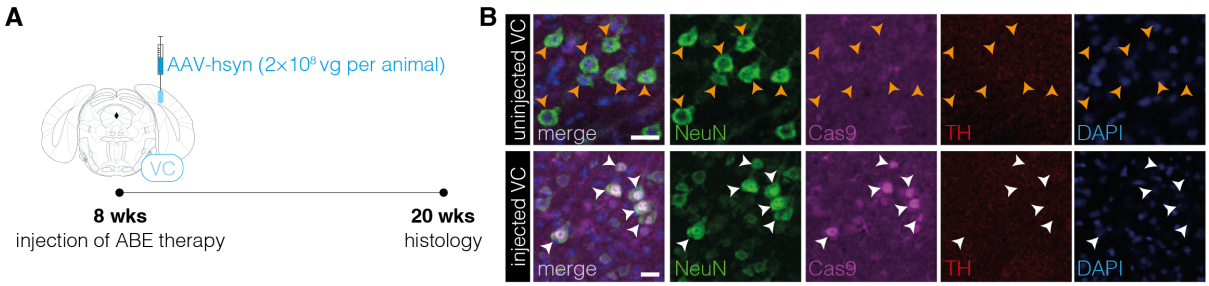


**Figure 3 – figure supplement 5 | Absence of TH$^+$ cell bodies in the visual cortex after neuronal PTBP1 downregulation. (A)** Schematic representation of the experimental timeline and setup. **(B)** Representative images showing ABE8e expression in neurons (white arrowheads) of the visual cortex (VC) in the injected hemisphere and absence of TH$^+$ cell bodies after 12 weeks (bottom). Absence of ABE8e expression in neurons (orange arrowheads) of the uninjected hemisphere (top) is shown for comparison (n=3 mice). Scale bars, 20μm. VC, visual cortex; NEUN, hexaribonucleotide binding protein-3; Cas9, *Streptococcus pyogenes* Cas9; TH, tyrosine hydroxylase; DAPI, 4',6-diamidino-2-phenylindole.

bioRxiv preprint doi: https://doi.org/10.1101/2024.03.22.586274; this version posted October 8, 2024. The copyright holder for this preprint (which was not certified by peer review) is the author/funder, who has granted bioRxiv a license to display the preprint in perpetuity. It is made available under aCC-BY 4.0 International license.

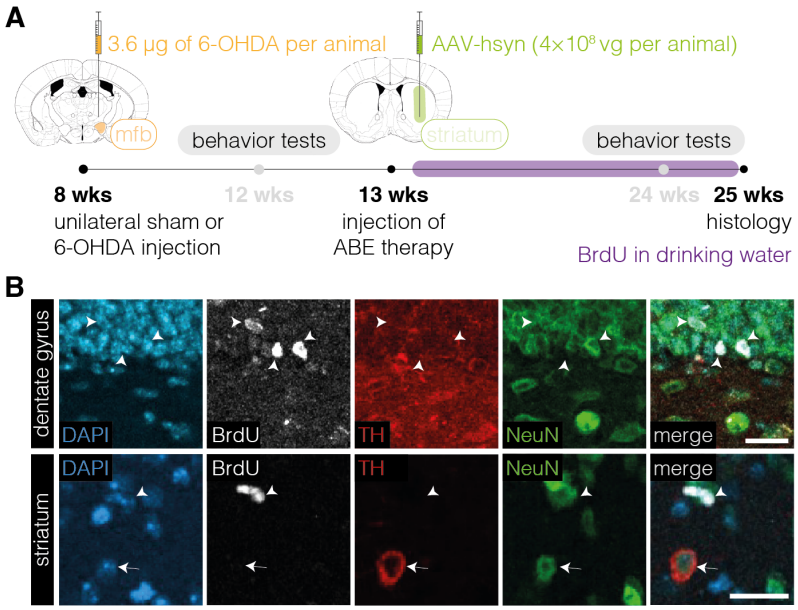


**Figure 3 – figure supplement 6 | Absence of proliferation in TH$^+$ cell bodies in the striatum after neuronal PTBP1 downregulation. (A)** Schematic representation of the experimental timeline and setup. (**B**) Representative images of BrdU-labeled cells (white arrowhead) in the dentate gyrus (DG, top) or striatum (bottom) and of TH$^+$ cell bodies (white arrow) in the striatum of animals treated with AAV-hsyn (n=4 mice; n=163 TH$^+$ cell bodies in the striatum). Images of the DG are shown as a positive control (top). Scale bars, 20µm. ABE, adenine base editor; DAPI, 4',6-diamidino-2-phenylindole; BrdU, bromodeoxyuridine; TH, tyrosine hydroxylase; NEUN, hexaribonucleotide binding protein-3.

bioRxiv preprint doi: https://doi.org/10.1101/2024.03.22.586274; this version posted October 8, 2024. The copyright holder for this preprint (which was not certified by peer review) is the author/funder, who has granted bioRxiv a license to display the preprint in perpetuity. It is made available under aCC-BY 4.0 International license.

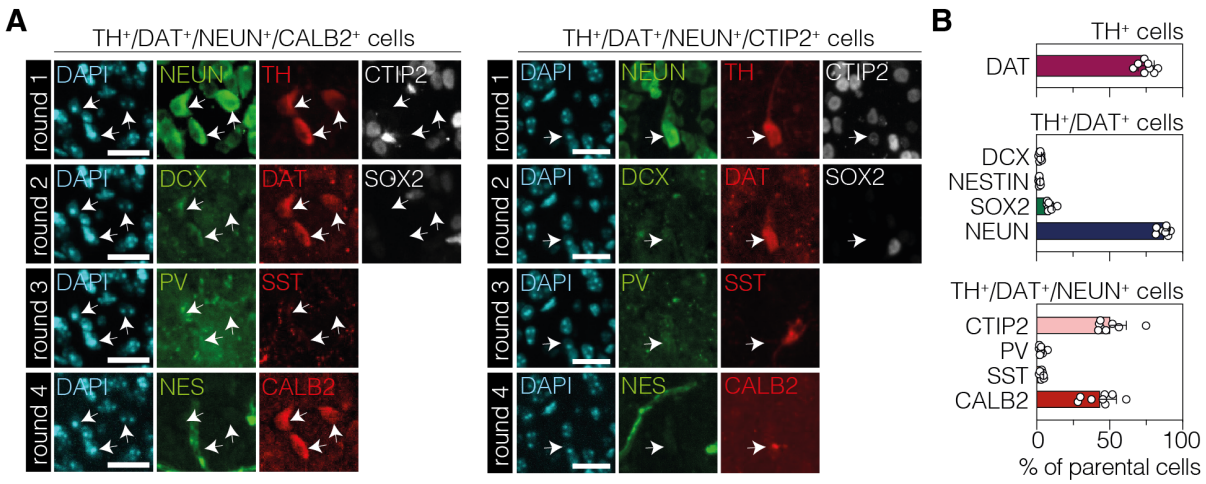


**Figure 4 | Characterization of TH$^+$ cells in the striatum after neuronal PTBP1 downregulation.** (**A**) Representative 4i images of the two main cell populations among TH-positive cells. The expressed markers are indicated on top of the images. (**B**) Corresponding quantifications of phenotypic markers expressed among TH-positive cells (top, DAT; n=696 TH$^+$ cells), TH/DAT double-positive (middle, DCX; NESTIN; SOX2; n=527 cells), or TH/DAT/NEUN triple-positive (bottom, CTIP2; PV; SST; CALB2; n=460 cells) subpopulations (white arrows) in the striatum at 12 weeks after administration of the AAV-hsyn treatment. The parental population is indicated above each plot. 4i imaging rounds are indicated on the left in (A). Images were pseudocolored during post-processing. Scale bars, 20μm. Data are displayed as means of 6 mice (B). DAPI, 4',6-diamidino-2-phenylindole; SOX2, sex determining region Y-box 2; NES, neuroepithelial stem cell protein; DCX, doublecortin; NEUN, hexaribonucleotide binding protein-3; TH, tyrosine hydroxylase; DAT, dopamine transporter; CTIP2, COUP-TF-interacting protein 2; PV, parvalbumin; SST, somatostatin; CALB2, calbindin 2.

bioRxiv preprint doi: https://doi.org/10.1101/2024.03.22.586274; this version posted October 8, 2024. The copyright holder for this preprint (which was not certified by peer review) is the author/funder, who has granted bioRxiv a license to display the preprint in perpetuity. It is made available under aCC-BY 4.0 International license.

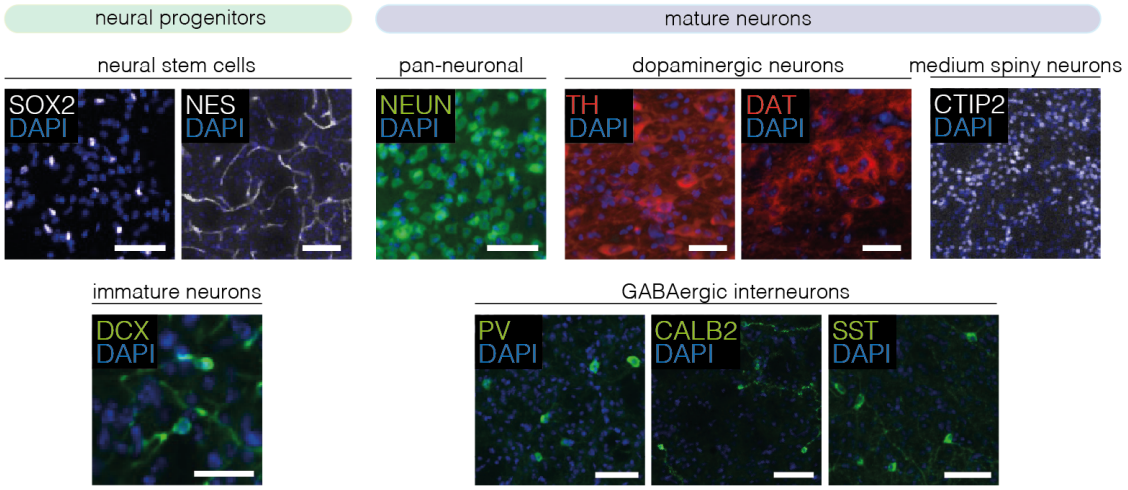


**Figure 4 – figure supplement 1 | Validation of antibodies for 4i experiments.** Antibody specificity was assessed on mouse brain sections of the striatum or SNc (n=2 animals). Representative images of one animal are shown. Scale bars, 50µm. DAPI, 4',6-diamidino-2-phenylindole; SOX2, sex determining region Y-box 2; NES, neuroepithelial stem cell protein; DCX, doublecortin; NEUN, hexaribonucleotide binding protein-3; TH, tyrosine hydroxylase; DAT, dopamine transporter; CTIP2, COUP-TF-interacting protein 2; PV, parvalbumin; CALB2, calbindin 2; SST, somatostatin.

bioRxiv preprint doi: https://doi.org/10.1101/2024.03.22.586274; this version posted October 8, 2024. The copyright holder for this preprint (which was not certified by peer review) is the author/funder, who has granted bioRxiv a license to display the preprint in perpetuity. It is made available under aCC-BY 4.0 International license.

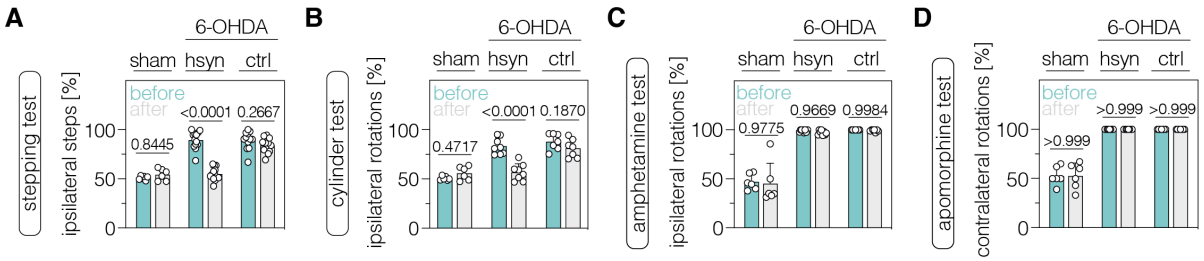


**Figure 5 | Neuronal PTBP1 downregulation in the striatum alleviates drug-free motor dysfunction in 6-OHDA-lesioned PD mice. (A,B)** Spontaneous behaviors, assessed as contralateral forelimb akinesia in the stepping test (A) and spontaneous rotations in the cylinder test (B), in animals treated in the striatum. (**C,D**) Drug-induced rotations, assessed as amphetamine-induced ipsilateral rotations (C) and apomorphine-induced contralateral rotations (D), in animals treated in the striatum. Normal distribution of the data was analyzed using the Shapiro-Wilk test. Data are represented as means±s.d. of 6-13 animals per group and were analyzed using a two-way ANOVA with Śidák's multiple comparisons. Each datapoint represents one animal. Exact *P*-values are indicated in each plot. hsyn, AAV-hsyn-ABE treatment; ctrl, AAV-ctrl-ABE treatment.

bioRxiv preprint doi: https://doi.org/10.1101/2024.03.22.586274; this version posted October 8, 2024. The copyright holder for this preprint (which was not certified by peer review) is the author/funder, who has granted bioRxiv a license to display the preprint in perpetuity. It is made available under aCC-BY 4.0 International license.

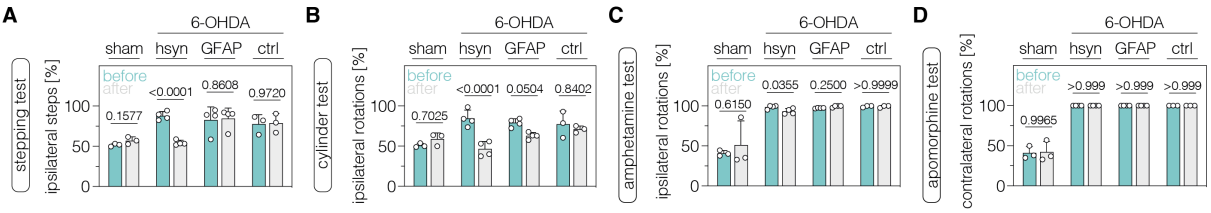


**Figure 5 – figure supplement 1 | Neuronal PTBP1 downregulation in the SNc alleviates drug-free motor dysfunction in 6-OHDA-lesioned PD mice. (A,B)** Spontaneous behaviors, assessed as contralateral forelimb akinesia in the stepping test (A) and spontaneous rotations in the cylinder test (B), in animals treated in the SNc. (**C,D**) Drug-induced rotations, assessed as amphetamine-induced ipsilateral rotations (C) and apomorphine-induced contralateral rotations (D), in animals treated in the SNc. Normal distribution of the data was analyzed using the Shapiro-Wilk test. Data are represented as means±s.d. of 3-4 animals per group and were analyzed using a two-way ANOVA with Śidák's multiple comparisons test. Each datapoint represents one animal. Exact *P*-values are indicated in each plot. hsyn, AAV-hsyn-ABE treatment; GFAP, AAV-GFAP-ABE treatment; ctrl, AAV-ctrl-ABE treatment.

bioRxiv preprint doi: https://doi.org/10.1101/2024.03.22.586274; this version posted October 8, 2024. The copyright holder for this preprint (which was not certified by peer review) is the author/funder, who has granted bioRxiv a license to display the preprint in perpetuity. It is made available under aCC-BY 4.0 International license.

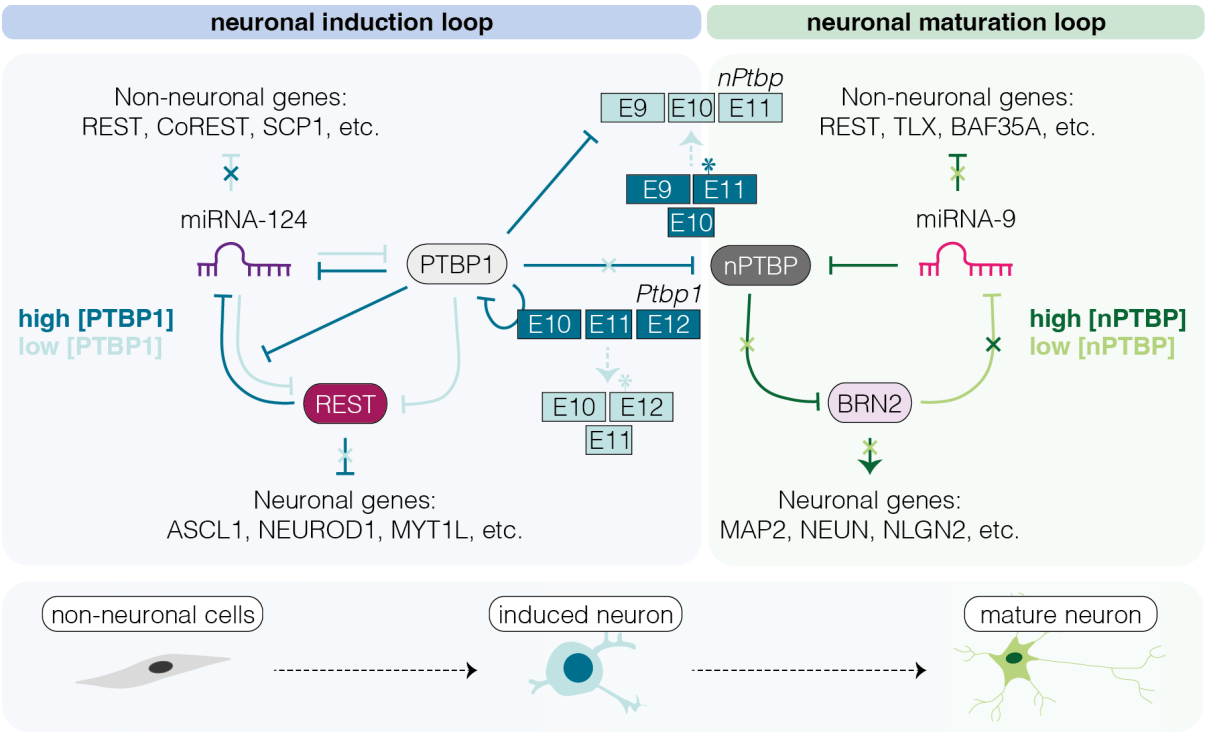


**Figure 5 – figure supplement 2 | Schematic representation of the PTBP1/nPTBP regulatory loops driving neuronal differentiation and maturation.** The dynamic regulation of PTBP1-mediated inhibition of miRNA-124, which acts on components of the REST complex to activate neuronal-specific expression programs in non-neuronal cells is a key event in the miRNA-124/REST signaling cascade. High PTBP1 expression in non-neuronal cells blocks miRNA-124-induced neuronal differentiation. During neuronal differentiation (low [PTBP1]), miRNA-124 represses PTBP1, enabling expression of nPTBP, pro-neuronal transcription factors, and consequently neuron-specific splicing events that eventually lead to neuronal maturation (Makeyev et al., 2007; Xue et al., 2013).

bioRxiv preprint doi: https://doi.org/10.1101/2024.03.22.586274; this version posted October 8, 2024. The copyright holder for this preprint (which was not certified by peer review) is the author/funder, who has granted bioRxiv a license to display the preprint in perpetuity. It is made available under aCC-BY 4.0 International license.

# Supplementary tables

Supplementary table 1: Oligos used for cloning of sgRNA plasmids.

| oligo name | sgRNA_ID | sequence (5′ → 3′) |
|---|---|---|
| sgRNA01_PTBP1_fwd | sgRNA-01 | CACCGACTTACCCGTCCATGGCACA |
| sgRNA01_PTBP1_rev | | AAACTGTGCCATGGACGGGTAAGTC |
| sgRNA02_PTBP1_fwd | sgRNA-02 | CACCGCTTACCTGCTGAGGCAGAGC |
| sgRNA02_PTBP1_rev | | AAACGCTCTGCCTCAGCAGGTAAGC |
| sgRNA03_PTBP1_fwd | sgRNA-03 | CACCGTTCTCAGCGGGGATCCGACG |
| sgRNA03_PTBP1_rev | | AAACCGTCGGATCCCCGCTGAGAAC |
| sgRNA04_PTBP1_fwd | sgRNA-04 | CACCGACTCACCAGCTTGGCATGCT |
| sgRNA04_PTBP1_rev | | AAACAGCATGCCAAGCTGGTGAGTC |
| sgRNA05_PTBP1_fwd | sgRNA-05 | CACCGCCCACAGTCCCTGGATGGCC |
| sgRNA05_PTBP1_rev | | AAACGGCCATCCAGGGACTGTGGGC |
| sgRNA06_PTBP1_fwd | sgRNA-06 | CACCGCTTACCAAAGGCTGCTGCCA |
| sgRNA06_PTBP1_rev | | AAACTGGCAGCAGCCTTTGGTAAGC |
| sgRNA07_PTBP1_fwd | sgRNA-07 | CACCGAATACCTGCGGCCTGAGGGA |
| sgRNA07_PTBP1_rev | | AAACTCCCTCAGGCCGCAGGTATTC |
| sgRNA08_PTBP1_fwd | sgRNA-08 | CACCGACATACCTCAGGGTTCAGAT |
| sgRNA08_PTBP1_rev | | AAACATCTGAACCCTGAGGTATGTC |

Supplementary table 2: Oligos used for cloning of AAV plasmids.

| oligo name | sequence (5′ → 3′) |
|---|---|
| pGfap-AAV-fwd | CGGCCTCTAGATCAGGGTACCAACATATCCTGGTGTGGAGTAGGG |
| pGfap-AAV-rev | CGGCCTCTAGATCAGGGTACCAACATATCCTGGTGTGGAGTAGGG |
| phsyn-AAV-fwd | CGGCCTCTAGATCAGGGTACCGAGGGCCCTGCGTATGAG |
| phsyn-AAV-rev | CTGTCCGTTTCATGGTGGCACCGGTCCAACTCTCGACTGCGCTC |

Supplementary table 3: Oligos used for RT-qPCR.

| oligo name | sequence (5′ → 3′) |
|---|---|
| Gapdh-RTqPCR_fwd | CATCACTGCCACCCAGAAGACTG |
| Gapdh-RTqPCR_rev | ATGCCAGTGAGCTTCCCGTTCAG |
| Ptbp1-RTqPCR_fwd | CACCGCTTCAAGAAACCAGGCT |
| Ptbp1-RTqPCR_rev | GTTGCTGGAGAAGAGGCTCTTG |
| Ptbp2-RTqPCR_fwd | CCTGTAACACTTGATGTCCTTCAC |
| Ptbp2-RTqPCR_rev | CACCATACTGGAGCAAAGCCTG |
| Ptbp3-RTqPCR_fwd | CTCGCTGGTTTCCCGGAG |
| Ptbp3-RTqPCR_rev | TCCCCGCTTTAAACCGACTG |
| Kcnq2-RTqPCR_fwd | GTCTTCTCCTGCCTTGTGCT |
| Kcnq2-RTqPCR_rev | GCAGCCCAGATCCTCACAAA |

Supplementary table 4: List of antibodies used in this study.

| antibody | clone | host species | dilution | application |
|---|---|---|---|---|
| NEUN | EPR12763 | rabbit | 1:1′000 | histology, primary |
| GFAP | ab95231 | chicken | 1:1′500 | histology, primary |
| TH | na | mouse | 1:1′000 | histology&4i, primary |
| TH | ab76442 | chicken | 1:500 | histology, primary |
| *Sp*Cas9 | 7A9-3A3 | mouse | 1:50 | histology, primary |
| BrdU | BU1/75 (ICR1) | rat | 1:400 | histology, primary |
| DCX | sc-8066 | goat | 1:300 | 4i, primary |
| Nestin | EPR22023 | rabbit | 1:100 | 4i, primary |
| Sox2 | 14-9811-82 | rat | 1:300 | 4i, primary |
| DAT | ab184451 | rabbit | 1:300 | 4i, primary |
| CTIP2 | 25B6 | rat | 1:500 | 4i, primary |
| PV | EPR13091 | goat | 1:100 | 4i, primary |
| SST | G10 | mouse | 1:250 | 4i, primary |
| CALB2 | 6B3 | mouse | 1:250 | 4i, primary |
| anti-rabbit AF488 | JIR-711-545-152 | donkey | 1:1′000 | histology, secondary |
| anti-rabbit Cy3 | JIR-711-165-152 | donkey | 1:500 | histology, secondary |

bioRxiv preprint doi: https://doi.org/10.1101/2024.03.22.586274; this version posted October 8, 2024. The copyright holder for this preprint (which was not certified by peer review) is the author/funder, who has granted bioRxiv a license to display the preprint in perpetuity. It is made available under aCC-BY 4.0 International license.

Supplementary table 4 continued.

| antibody | clone | host species | dilution | application |
|---|---|---|---|---|
| anti-chicken Cy5 | JIR-703-175-155 | donkey | 1:500 | histology, secondary |
| anti-mouse Cy3 | JIR-715-165-151 | donkey | 1:500 | histology, secondary |
| anti-goat AF488 | JIR-705-545-003 | donkey | 1:1'000 | histology, secondary |
| anti-goat Cy5 | JIR-705-175-147 | donkey | 1:5000 | histology, secondary |
| anti-rat Cy5 | JIR-712-175-153 | donkey | 1:500 | histology, secondary |
| PTBP1 | EPR9048B | rabbit | 1:10'000 | Western blot, primary |
| ACTB | ab8226 | mouse | 1:2'000 | Western blot, primary |
| IRDye® 680RD anti-rabbit IgG | 926-68073 | donkey | 1:20'000 | Western blot, secondary |
| IRDye® 800CW anti-mouse IgG | 926-32212 | donkey | 1:20'000 | Western blot, secondary |

Supplementary table 5: Oligos used for deep sequencing.

| oligo name | sequence (5' → 3') |
|---|---|
| PTBP1.ex1-HTS_fwd | CTTTCCCTACACGACGCTCTTCCGATCTNNNNNNTTCTGCTATTCCTGCGCCTC |
| PTBP1.ex1-HTS_rev | GGAGTTCAGACGTGTGCTCTTCCGATCTNNNNNNCATTGCAGCGGTTAGAGGGA |
| PTBP1.ex3-HTS_fwd | CTTTCCCTACACGACGCTCTTCCGATCTNNNNNNTGCAAATGGGAATGCAGGAA |
| PTBP1.ex3-HTS_rev | GGAGTTCAGACGTGTGCTCTTCCGATCTNNNNNNCAGGTCCTTTCTCCCAGCTC |
| PTBP1.ex7.1-HTS_fwd | CTTTCCCTACACGACGCTCTTCCGATCTNNNNNNATGCCAAGCTGGTGAGTAGG |
| PTBP1.ex7.1-HTS_rev | GGAGTTCAGACGTGTGCTCTTCCGATCTNNNNNNGCAGGTCAGGTCGAGTGTAG |
| PTBP1.ex7.2-HTS_fwd | CTTTCCCTACACGACGCTCTTCCGATCTNNNNNNCTACACTCGACCTGACCTGC |
| PTBP1.ex7.2-HTS_rev | GGAGTTCAGACGTGTGCTCTTCCGATCTNNNNNNATCACTGCACCTCACCTCAC |
| PTBP1.ex8-HTS_fwd | CTTTCCCTACACGACGCTCTTCCGATCTNNNNNNGTCAGCCTCTCCGTATGCAG |
| PTBP1.ex8-HTS_rev | GGAGTTCAGACGTGTGCTCTTCCGATCTNNNNNNCCTGTGGATGCTTCTGGAGG |
| PTBP1.ex9-HTS_fwd | CTTTCCCTACACGACGCTCTTCCGATCTNNNNNNGGTGCTGGGAATTCTGTCCT |
| PTBP1.ex9-HTS_rev | GGAGTTCAGACGTGTGCTCTTCCGATCTNNNNNNCAGCAGTGGCAGATAGAGGG |
| Mypn1_HTS_fwd | CTTTCCCTACACGACGCTCTTCCGATCTNNNNNNGGTCAAAAATGGCGCAAGGT |
| Mypn1_HTS_rev | GGAGTTCAGACGTGTGCTCTTCCGATCTNNNNNNTGCACACACTGACAAGGACT |
| Ank1_HTS_fwd | CTTTCCCTACACGACGCTCTTCCGATCTNNNNNNTGTTTTCTGCTTCTCAGGGGA |
| Ank1_HTS_rev | GGAGTTCAGACGTGTGCTCTTCCGATCTNNNNNNCAGTGGTCCAAGACCGTACA |

Supplementary table 6: Reference nucleotide sequences of amplicons for deep sequencing.

| amplicon name | amplicon sequence (5'→ 3') |
|---|---|
| PTBP1.ex1 | TTCTGCTATTCCTGCGCCTCCGCTCCGTTCCCCGCGGGTCTCTTCCGTGTGCCATGGA<br>CGGGTAAGTCCTGCCGCGCCCCTCGCACGCCGCTCCGCTCACCACTCCGTCCCAGCCA<br>TCGCTGCCGCGCGCGTGGACTTTTGGCCCCCGCCGATCCCTCTAACCGCTGCAATG |
| PTBP1.ex3 | TGCAAATGGGAATGCAGGAAAGGAATCAGCCTGGAACTAAGATTCCATGCTCTCTTCT<br>CAGCGGGGATCCGACGAGCTCTTCTCCACGTGTGTCAGCAACGGCCCCTTCATCATGA<br>GCAGCTCTGCCTCAGCAGGTAAGAGTGCCTGGGTGCCCTAGGGAGTCCTGCCTTGACA<br>GGTACAGGGCGAGCTGGGAGAAAGGACCTG |
| PTBP1.ex7.1 | ATGCCAAGCTGGTGAGTAGGACTTGCTTGGGTGGGCAATCCTATGACTGGCCCACGCA<br>CTCACCTATGGCTCCCCACAGTCCCTGGATGGCCAGAACATCTACAACGCCTGCTGCA<br>CGCTGCGCATCGACTTCTCCAAGCTCACCAGTCTCAATGTCAAGTACAACAATGATAA<br>GAGCAGAGACTACACTCGACCTGACCTGC |
| PTBP1.ex7.2 | CTACACTCGACCTGACCTGCCCTCTGGAGACAGCCAGCCTTCACTAGACCAGACCATG<br>GCAGCAGCCTTTGGTAAGATGCTGTACTGAGACACACCAAATGAACAGGGGTGGGACA<br>GGCCACCTAGCTGTCAGGGCACCCTGGCACTGCACAGCCCAGCCACTCAGCAGTCCTG<br>CCCGTGCCTGGCCCAGCCGTGAGGTGAGGTGCAGTGAT |
| PTBP1.ex8 | GTCAGCCTCTCCGTATGCAGGAGCCGGGTTCCCTCCCACCTTTGCCATCCCTCAGGCC<br>GCAGGTATTCACGCTCATCCTGACCCCAGCGCCTGCATGCCCACACAGCCCCATAACT<br>GTCCATAGACCGGGATGCCACTGGCCCCAAGTGTTAGGCCCCAGGCCCCCTTCCTTCT<br>GGGGAGAGGGGAAGGGGCCTCCAGAAGCATCCACAGG |
| PTBP1.ex9 | GGTGCTGGGAATTCTGTCCTTTTGGTCAGCAATCTGAACCCTGAGGTATGTGGGTATT<br>GCTGTGCTCTGCTTATACATGGAGTAGTGGTGGGGTGCTGACTGACCACAAGTCAGGG<br>TGGGGGAGCATACTGGATGGCAAGCAGGGTTTCTGGGTGTCCCAGGCGCCGTGTGGGT<br>ATAGGCGTGCTGCCCCTCTATCTGCCACTGCTG |

bioRxiv preprint doi: https://doi.org/10.1101/2024.03.22.586274; this version posted October 8, 2024. The copyright holder for this preprint (which was not certified by peer review) is the author/funder, who has granted bioRxiv a license to display the preprint in perpetuity. It is made available under aCC-BY 4.0 International license.

| amplicon name | amplicon sequence (5′→ 3′) |
|---|---|
| Mypn-OT1 | GGTCAAAAATGGCGCAAGGTCAGAGGGCACCGTGGGTTCCAGCACACCTGCCCGCAGC GCTTCATCCATAGGCCCTGAGCTACCACCCAGCTCTGCTTCAGCAGGTACCCAGTACA GCTTGAGGTCAGCAGCTTGCTCCCATGCCTGTTCTTTGCTTTGCAAATGAGTCCTTGT CAGTGTGTGCA |
| Ank1-OT2 | TGTTTTCTGCTTCTCAGGGGAGAATCAGCTGTTCTGGCCATTTGATGGTACAGGGTTT GCCCATTCGAAGCCGACTCAGCCCTGCTCTGTCTCACAGGTAAGCACACGAGATCCCC CTTTTCTGGAGCCCTCCAGCGACCCCACTCACCACAGTGAACAGAAGTTGTACGGTCT TGGACCACTG |

1364

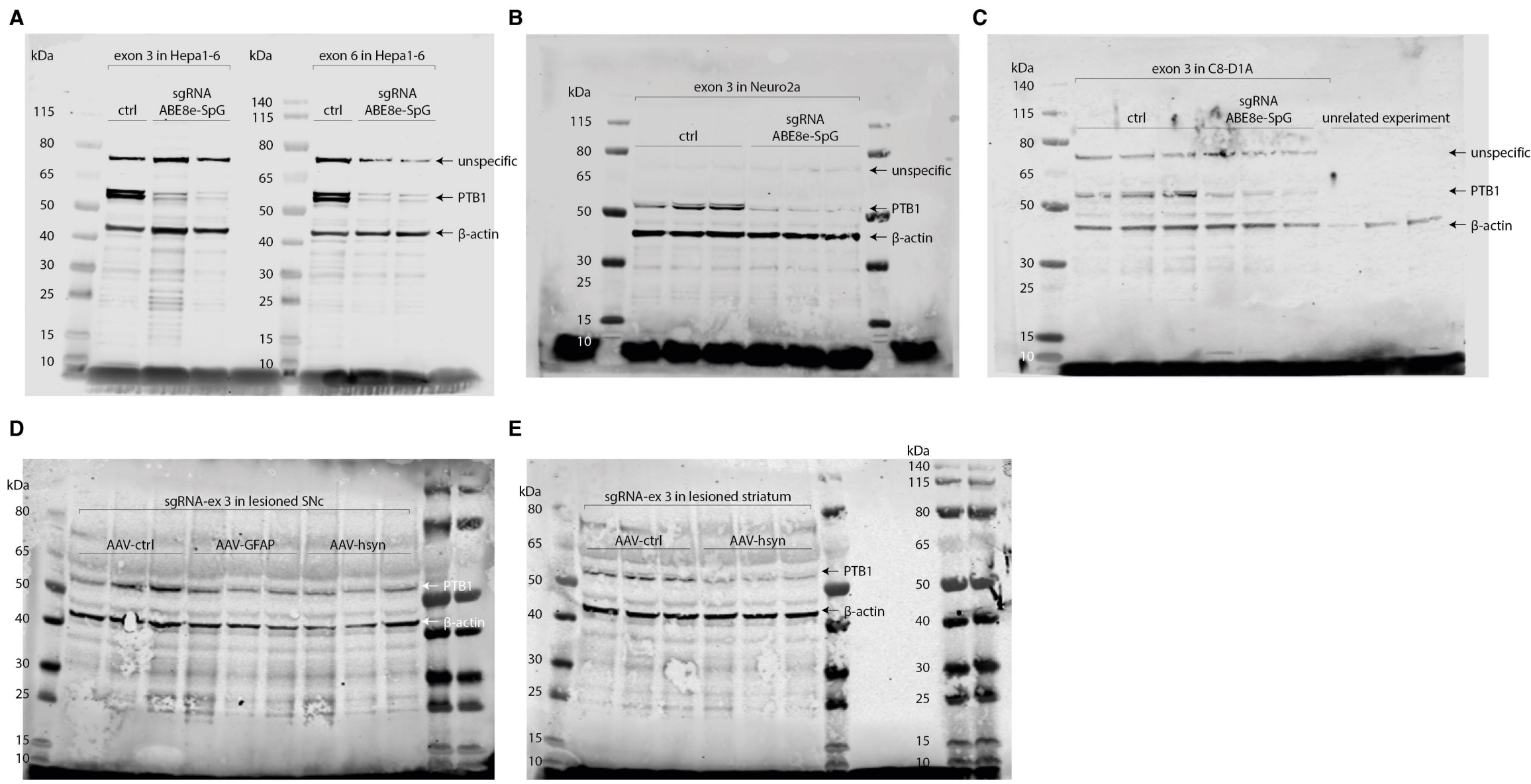
A
kDa
exon 3 in Hepa1-6
ctrl
sgRNA ABE8e-SpG
115
80
65
50
40
30
25
15
10
kDa
exon 6 in Hepa1-6
ctrl
sgRNA ABE8e-SpG
140
115
80
65
50
40
30
25
15
10
unspecific
PTB1
β-actin
B
kDa
exon 3 in Neuro2a
ctrl
sgRNA ABE8e-SpG
115
80
65
50
30
25
15
10
unspecific
PTB1
β-actin
C
kDa
exon 3 in C8-D1A
ctrl
sgRNA ABE8e-SpG
unrelated experiment
140
115
80
65
50
30
25
15
10
unspecific
PTB1
β-actin
D
kDa
sgRNA-ex 3 in lesioned SNc
AAV-ctrl
AAV-GFAP
AAV-hsyn
80
65
50
40
30
25
15
10
PTB1
β-actin
E
kDa
sgRNA-ex 3 in lesioned striatum
AAV-ctrl
AAV-hsyn
80
65
50
40
30
25
15
10
PTB1
β-actin
kDa
140
115
80
65
50
40
30
25
15
10